Modelling and multi-objective optimisation of heat transfer characteristics and pressure drop of nanofluids in microtubes

Marcel Meyer, Mehdi Mehrabi, Josua Petrus Meyer

Department of Mechanical and Aeronautical Engineering, University of Pretoria, Pretoria, Private Bag X20, Hatfield 0028, South Africa.

Address correspondence to Dr Mehdi Mehrabi, Department of Mechanical and Aeronautical Engineering, University of Pretoria, Private Bag X20, Hatfield, Pretoria, 0028, South Africa. E-mail: mehdi.mehrabi@up.ac.za Phone Number: (+27) 12 420 4743, Fax Number: (+27) 12 420 6632.

ABSTRACT

Multi-objective optimisation of nanofluids in a microchannel heat sink was conducted to determine the highest Nusselt number and the lowest pressure drop. This was done by creating a design study consisting of four nanoparticles of Al_2O_3, CuO, ZnO and SiO_2 with four diameters of 10, 30, 60 and 100 nm, nanoparticle volumetric concentrations of 0.001, 0.005, 0.01 and 0.05 and four base fluids of water (W), ethylene glycol (EG), W/EG (50/50) and W/EG (60/40). Every possible combination of these four input parameters created 256 design points for the numerical simulation. The outcome of the numerical simulation depended on the performance of heat transfer and pressure drop. A modified non-dominated sorting genetic algorithm was then used to determine the highest Nusselt number and the lowest pressure drop based on the numerical results of the 256 design points. The outcome of the optimisation was that silicon dioxide-water (SiO_2) nanofluid gave the optimal combination of heat transfer and pressure drop. The results also showed that the nanoparticle diameter had a small effect on the pressure drop in the microchannel heat sink and an increase in the nanoparticle volumetric concentration increased the heat transfer coefficient.

INTRODUCTION

The enhancement of the thermal conductivity of cooling systems has been of interest since Choi and Eastman [1] published an article in 1995 on the concept of adding nanoparticles to the working fluid to achieve a higher thermal conductivity [2]. This new working fluid was named nanofluid. A nanoparticle can be metal, metal oxide or carbon nanotube. This new working fluid has one or a combination of different types of particles prepared to a small size of nanometre. The downside of using nanofluids instead of conventional working fluids is the increase of pressure drop (pumping power needed) [3].

Tuckerman and Pease [4] were the first to introduce the concept of adding channels to a heat sink and forcing coolant over the channels. They realised that the heat transfer coefficient had a reverse proportionality to the width of the channels. Xue et al. [5] report that the heat transfer enhancement of parallel channels is due to the shortened flow length. An experimental and numerical study by Lee et al. [6] showed that the numerical results were in good agreement with the experimental results proving that microchannels could be solved numerically as well. Fluid flow and heat transfer simulation inside microchannels has also received some attention as Foong et al. [7] have shown by developing an empirical formula for the Nusselt number using functions of axial distance. From the literature, it can be concluded that the microchannels enhance the heat transfer; however, the addition of microchannels is not the only means of achieving higher heat transfer rates.

Modification of the heat transfer fluid is currently possible due to the increased technology of nanofluid preparation. A nanofluid is made by dispersion of nanosized particles in a base fluid. Properties of nanofluids have been a topic of different views and results and the models developed

for property characterisation of nanofluids have yielded different results. Prasher et al. [8] conclude that the viscosity of nanofluids depends on nanoparticle diameter, volumetric concentration, temperature as well as shear rate. Xuan et al. [9] mention that particle aggregation is still a problem with nanofluids losing its efficacy over long periods of time. They also discovered that a copper nanoparticle and water combination yielded higher thermal conductivity compared with the conductivity of the base fluid alone. The volumetric concentration of nanoparticles was investigated by Anoop et al. [10]. They reviewed the nanofluid literature and concluded that there was no approach that showed the change of thermal conductivity when a nanoparticle was added to the base fluid. Disagreements in the field are still evident. However, the focus of this study is not on the nanofluid properties but on the effect of nanofluid properties on the heat transfer characteristics and pressure drop.

Nanofluids in conjunction with microchannels then seemed to be the next step of heat transfer enhancement of systems. Kahani [11] conducted a study on the effect of the modern dispersion model on nanofluids through microchannels and concluded that decreasing the nanoparticle diameter as well as increasing the nanoparticle volumetric concentration enhanced the heat transfer coefficient. Coşkun and Çetkin [12] also showed that the addition of nanoparticles with micro pin fins maximised the thermal conductivity. The introduction of ellipse and diamond ribs inside a microchannel using Al_2O_3-water nanofluids was studied by Abdollahi et al. [13]. Their results showed that if a 2% volumetric concentration of nanoparticles was used, the ellipse ribs produced better heat transfer results than the diamond ribs or no ribs at all.

With the advancement of soft computing methods, numerical simulations, and optimisation algorithms, these have been used in the heat transfer community as well. Some of the preferred methods are neural networks and genetic algorithms. As can be seen in the work of Tam et al. [14],

the pattern recognition of empirical data is one of the strengths of the soft computing methods. Soft computing methods can be used to predict certain heat transfer characteristics. Mehrabi et al. [15] studied multi-objective optimisation of the heat transfer and pressure drop of titanium dioxide-water nanofluids and showed that these methods could predict the Nusselt numbers and pressure drops in agreement with the experimental results.

A review of the literature revealed that no multi-objective optimisation of a nanofluid in a microchannel with regard to the heat transfer and pressure drop has been conducted. This study set out to determine the optimal input parameters of a nanoparticle and its diameter, nanoparticle volumetric concentration, its base fluid using a modified non-dominated sorting genetic algorithm (NSGA) for the optimum combined outcomes of heat transfer and pressure drop. The emphasis was on having the highest possible Nusselt number and the lowest pressure drop. Included in the current research work was the set-up of a numerical model able to automatically take the input parameters, create a design study based on the possible combinations of various input parameters and then determine the optimal combination. This was to ensure that continued study could be done with the use of the model.

NUMERICAL MODEL

Geometry

The microchannel geometry has a significant effect on the overall heat transfer performance of a microchannel. The optimisation criterion of this study was to find the lowest pressure drop while having the highest Nusselt number based on the best possible combination of four input parameters. Therefore, if the effect of input parameters was to be analysed, the geometry had to remain constant. The configuration of microchannels differs from design to design. Chein and

Chen [16] studied the effects of the inlet outlet configuration of a microchannel. Their study concluded that the V-type inlet with fluid flow entering and leaving vertically resulted in the largest heat transfer. Therefore, a microchannel with a V-type inlet used by Chein and Chen [16] and Abdollahi et al. [17] was selected for this study. The model was recreated in Solidworks [version 2018] and used throughout the simulation and design study. Figures 1 (a), (b) and (c) show the details of the microchannel geometry and microchannel dimensions.

Governing equations

Assumptions for the model and numerical simulations were as follows:

1) steady state;
2) *k*-ε turbulent model with enhanced wall functions;
3) Newtonian fluid;
4) nanoparticle and base fluid are in thermal equilibrium;
5) single phase;
6) the properties of fluid flow and the microchannel are constant and temperature independent.

Enhanced wall functions were used due to a coarse mesh near the walls as this mesh was needed to ensure a smaller total mesh count. This function was highly recommended because the y^+ value was bigger than 15. The Ansys Theory Guide [18] recommends using the *k*-ε turbulence model with enhanced wall functions. Following the assumptions, the governing equations could be set out and used in Ansys [Version 2019 R2]. All these equations were used for water and nanofluids because the fluids behaved in the same way.

Continuity:

$$\nabla \cdot \vec{V} = 0 \tag{1}$$

Momentum equation:

$$\rho\left(\vec{V} \cdot \nabla \cdot \vec{V}\right) = -\nabla p + \mu \nabla^2 \vec{V} \tag{2}$$

Energy equation for fluid flow:

$$\rho C_p\left(\vec{V} \cdot \nabla T\right) = \mathrm{k}\nabla^2 \vec{V} \tag{3}$$

Energy equation for solid section (the microchannel itself):

$$\mathrm{k_s}\nabla^2 T_s = 0 \tag{4}$$

From the turbulence model, two extra equations were added to calculate the turbulence.

Turbulent kinetic energy (*k*):

$$\frac{\partial(\rho k)}{\partial t} + \frac{\partial(\rho k u_i)}{\partial x_i} = \frac{\partial}{\partial x_j}\left[\frac{\mu_t}{\sigma_k}\frac{\partial k}{\partial x_j}\right] + 2\mu_t E_{ij} E_{ij} - \rho\varepsilon \tag{5}$$

Turbulent kinetic energy dissipation rate (ε):

$$\frac{\partial(\rho\varepsilon)}{\partial t} + \frac{\partial(\rho\varepsilon u_i)}{\partial x_i} = \frac{\partial}{\partial x_j}\left[\frac{\mu_t}{\sigma_\varepsilon}\frac{\partial \varepsilon}{\partial x_j}\right] + C_{1\varepsilon}\frac{\varepsilon}{k}2\mu_t E_{ij} E_{ij} - C_{2\varepsilon}\rho\frac{\varepsilon^2}{k} \tag{6}$$

$$\mu_t = \rho C_\mu \frac{k^2}{\varepsilon} \tag{7}$$

where u_i, E_{ij}, μ_t are the velocity component in the corresponding direction, the component of rate of deformation and the eddy viscosity, respectively.

Reynolds number:

$$Re = \frac{\rho u_{ave} D_h}{\mu} \tag{8}$$

Nusselt number:

$$Nu = \frac{h(x) D_h}{k} = \frac{q_w D_h}{k(T_w - T_b)} \tag{9}$$

$$Nu = \frac{h D_h}{k} = \frac{q_w D_h}{k(T_{hs} - T_{ave})} \tag{10}$$

Pressure drop:

$$\Delta p = \frac{1}{2} \rho F Q^2 \tag{11}$$

Mesh analysis

Mesh independence was measured with the grid convergence index (GCI) method specified in Roache [19]. This method uses a performance parameter to determine if convergence has been achieved. The average temperature in each channel of the microchannel was chosen to be the performance factor in this study because it could be compared with the results of Abdollahi et al. [17]. Performance factors were calculated and used to ensure that the value of the current mesh density was close to or the same as the mesh density of previous works. The following equation shows the correlation to calculate GCI:

$$GCI = \frac{F_s \left| \frac{f_2 - f_1}{f_1} \right|}{r^{pp} - 1} \tag{12}$$

If the GCI reaches 1, grid convergence is reached, and the mesh refinement can stop. This method works by analysing a chosen output parameter against the number of cells. If the outcome (in this study, the average temperature in each channel of the microchannel) does not change with an increase in the number of cells, it can be concluded that the mesh refinement can be stopped.

The GCI results of mesh independence are shown in Table 1. The outcome shows that if the number of cells is chosen to be 1 000 000, the convergence index reaches 1, showing that mesh independence has been achieved.

A mesh with 1 000 000 cells was used for this study and was simulated at the Centre for High Performance Computing in Cape Town [20]. This was done to ensure that there were no computational power constraints because the centre allocates 100 cores of CPU (Intel Xeon/2.6 GHz) to a user. The created mesh is shown in Figures 2 and 3.

Results of present numerical simulations with water and nanofluids as the working fluids

In this section, a comparison between the numerical results of Chein and Chen [16], Abdollahi et al. [17] and the present work is presented. The first iteration of the model was used with water as a base fluid for validation with Chein and Chen [16] because they only worked with water. Figure 4 indicates the numerical results of the temperature distribution of both Chein and Chen [16] and Abdollahi et al. [17]. The comparison with the present work is displayed in Figure 5.

To determine what measure or error was made between the different mesh qualities, the average temperature in each channel was compared. This gives a good indication of the overall validation of the presented numerical simulation. Figure 6 shows the comparison between the results of Chein and Chen [16], Abdollahi et al. [17] and the present work for the average temperature of water in different channels of the microchannel. The figure indicates that the maximum error was 1 K or 1.5% error. This validation of the results with the results of the other researchers ensured that the set-up of the present numerical simulation was done correctly. Chein and Chen [16] compared their computed local Nusselt numbers in the fifth channel of an I-type heat sink with that of Philips [21]. Their reported results showed a good agreement with the Philips [21]. This comparison helps

to confirm the validation of the geometry, meshing and the general assumptions and boundary conditions of the presented numerical simulation. A comparison of the maximum errors for the average temperature of each channel in the microchannel of the present work with those of Chein and Chen [16] and Abdollahi et al. [17] is given in Table 2.

A cross-section of the microchannel is also shown in Figure 7 to display the flow field inside each individual channel. Figures 8 and 9 show that the velocity and pressure contours matched with what was expected, namely a high pressure at the inlet and a lower one at the outlet. The velocity contour had some exceptional quality and detail because the residuals for velocity in all three directions were down to 10^{-8}. The inlet can be clearly seen as well as the velocity trails left by each channel at the outlet.

Repeating the numerical simulation with different nanofluids as the working fluid was the next step of the process, with the model validation of water already done. The properties of nanofluids were added by using a user-defined function (UDF). This allows the user to insert any desired defined function into the Ansys Workbench as a replacement for the property. The UDF used in this study was based on the models explained by equations (13-17).

Thermal conductivity [22]:

$$\mathrm{k}_{eff} = \frac{\mathrm{k}_{np} + 2\mathrm{k}_f + 2\left(\mathrm{k}_{np} - \mathrm{k}_f\right)\phi}{\mathrm{k}_{np} + 2\mathrm{k}_f - \left(\mathrm{k}_{np} - \mathrm{k}_f\right)\phi}\mathrm{k}_f + 5 \times 10^4 \beta\phi\rho_{np}C_p\sqrt{\frac{K_B T}{\rho_{np} d_{np}}} f(T,\phi) \qquad (13)$$

where K_B is the Boltzmann constant (K_B = 1.380649×10^{-23} J/K).

To calculate $f(T,\phi)$, the following equation was used:

$$f(T,\phi) = (2.8217 \times 10^{-2}\phi - 3.91123 \times 10^{-3})\left(\frac{T}{T_o}\right) + (3.0669 \times 10^{-2}\phi - 3.91123 \times 10^{-3}) \quad (14)$$

Specific heat capacity [23]:

$$C_{p_{nf}} = \frac{(1-\phi)(\rho C_p)_f + \phi(\rho C_p)_s}{\rho_{nf}} \quad (15)$$

Density [24]:

$$\rho_{nf} = (1-\phi)\rho_f + \phi\rho_s \quad (16)$$

Viscosity [23]:

$$\mu_{brownian} = 5 \times 10^4 \beta \rho_f \phi \sqrt{\frac{K_B T}{2\rho_{np} d_{np}}}((-134.63 + 1722.3\phi) + (0.4705 - 6.04\phi)T) \quad (17)$$

The set-up of the numerical simulation was done in a laminar flow with low Reynolds number of 1 333 with silicone dioxide (SiO_2) as the nanofluid and a constant heat flux of 100 (W/cm^2). The same properties as used in Abdollahi et al. [17] were used for the water and the nanofluid. The values were also cross-referenced with CES software [25].

Figure 10 shows the comparison between the results of Abdollahi et al. [17] and the present work for the average temperatures of water and nanofluid (SiO_2) in different channels of the microchannel. The results of the present work in both cases of water and nanofluid as working fluid correlated with those of the previous work done by Chein and Chen [16] as well as those of Abdollahi et al. [17].

The base case simulation was then used as the foundation of the optimisation analysis. This means that the Ansys model was correctly implemented according to the validation data shown in Figures 6 and 10. Only the material properties would be changed. These parameters would then be

optimised to find the best possible set-up to ensure the highest heat transfer coefficient and the lowest pressure drop. To do so, the first step was to generate enough data points for the optimisation section. Therefore, the data preparation was done by using four nanoparticles of Al_2O_3, CuO, ZnO and SiO_2 with four diameters of 10, 30, 60 and 100 nm, nanoparticle volumetric concentrations of 0.001, 0.005, 0.01 and 0.05 and four base fluids of water (W), ethylene glycol (EG), W/EG (50/50) and W/EG (60/40). All possible combinations of these inputs led to a data set consisting of 256 unique design points that could be used for optimisation purpose, as shown in Table 3.

PREPARATION OF DATA FOR OPTIMISATION

Equations (13) to (17) were used to calculate the properties of nanofluids for all 256 combinations of input parameters based on the thermophysical properties of nanoparticles [17] and the base fluids [26] that are given in Tables 4 and 5. A data set was then created for the thermophysical properties of nanofluids. Table 6 shows this data set for Al_2O_3-water nanofluids with particle diameters of 10 nm. The density, viscosity and specific heat capacity were constants and could be added into the parameter system of the Ansys Workbench. However, the thermal conductivity was temperature dependent and changed throughout the system, which was then added into Ansys using a UDF. In Ansys, any parameter can be set as an output to visualise the influence of the system on the parameter. This methodology was used with the UDF. Once the UDF was added, the output was monitored, and hand calculations were made at different time steps to confirm the outcome.

The example shown in Table 6 is a snip of the design study. Each possible iteration could be inserted into Ansys because the volumetric concentration of nanoparticles was being varied and the rest of the inputs were constant.

Ansys then simulated the given data and produced an output of the Nusselt number and pressure difference. The Nusselt number was calculated inside each of the channels whereas the pressure difference was calculated from the entrance to the exit.

Data preparation outcome

This subsection discusses the results of the data preparation, namely the performance of the nanoparticles and base fluids as well as the influence of the volumetric concentration and nanoparticle diameter on the outcome in order to understand the trends present in the outcome. For the optimisation, an in-depth knowledge of the data was needed to ensure that the outcome was correct.

The first step in the analysis was examining how the different base fluids performed in the numerical simulations. This was done by plotting the Nusselt number against the pressure drop and separating the different base fluids, indicating the effect of the base fluids on the pressure and heat transfer coefficient. The data provided trends and information about the influence of each parameter on the two outcomes (pressure drop and Nusselt number). The outcome aimed to optimise the inputs to ensure the lowest pressure drop and the highest Nusselt number in the microchannel. The data provided an understanding of the outcome relating to the influence of each input. Figure 11 clearly indicates that water was the optimal base fluid because its Nusselt number was the highest and its pressure drop the lowest, making it the optimal for overall heat transfer and pressure drop performance efficiency. The indications seen in the initial post-processing were later

confirmed through the multi-objective optimisation algorithm as water was again the optimal base fluid. Therefore, the first comparison tests and figures had to confirm the outcome of the optimisation. The performance of ethylene glycol came as a surprise as the worst-performing base fluid. The apparent performance of the water was justified with the 60-40 water-ethylene glycol mixture having the second lowest pressure drop: however, producing a Nusselt number as high as water.

The following step was to have a closer look at the effect of the volumetric concentration of nanoparticles and the nanoparticle diameter on the outcome. Figure 12 shows that the concentration influenced the Nusselt number, this effect seemed to be exponential with volumetric concentration of 0.05 nanoparticle, but no clear correlation was seen with the other volumetric concentration values. This then indicated why an optimisation algorithm was needed to determine the optimal point.

The effect of the volumetric concentration of nanoparticles was shown when all the inputs were kept constant and only the concentration was changed. Figure 12 shows what was expected of the concentration: a saturation point was reached where the Nusselt number would not change even if the concentration was increased. However, the pressure drop increased extremely fast because the fluid then became entirely nanoparticle, losing its fluid properties.

The nanofluid with volumetric concentration of 0.05 had the highest Nusselt number, but an extremely high pressure drop, indicating the negative effect of 0.05 volumetric concentration of nanoparticles on the pumping efficiency. The 0.01 volumetric concentration of nanoparticle offered a better solution with an acceptable pressure drop and a high Nusselt number, close to that of the 0.05 volumetric concentration. Figure 13 shows the effect of the volumetric concentration of nanoparticles on the output variables of both the Nusselt number and pressure drop for SiO_2-

water nanofluid when the nanoparticle diameter was 100 nm. Figures 14 and 15 show the effect of the nanoparticle volumetric concentration on the pressure drops and the Nusselt numbers of Al_2O_3-water, CuO-water, SiO_2-water, and ZnO-water nanofluids when the nanoparticle diameter was 100 nm. Figures 16 and 17 show the effect of the choice of nanoparticle on the Nusselt number and pressure drop of nanofluids when the base fluid was water, nanoparticle diameter was 100 nm, and the volumetric concentration was 0.01 as well as the effect of the nanoparticle diameters on the Nusselt number and pressure drop of nanofluids for different base fluids. The concentration had a positive effect on the Nusselt number and pressure drop. Therefore, if optimisation had to be done on these results, a sensitivity analysis would determine the outcome. It was also indicated that the effect on the pressure drop was more drastic than that of the Nusselt number, meaning that a small drop in Nusselt number ensured a considerable drop in pressure. Therefore, a small compromise on heat transfer can result in a big gain in pumping efficiency.

Figure 16 shows that the influence of nanoparticle type on the Nusselt number was small; however, the change in the value of the pressure drop was significant. Therefore, the SiO_2-water nanofluid performed the worst with the highest pressure drop, while the difference between silicon dioxide and zinc oxide's Nusselt numbers was only 0.2. Accordingly, the expected results after the optimisation would show that the SiO_2 could be the optimal nanoparticle. The small loss in heat transfer compared with the gain that the decreased pressure drop offered was an acceptable compromise. Figure 17 shows that the nanoparticle diameter had little to no effect on the outcome of the pressure drop or Nusselt number. The conclusion that the diameter had an extremely small effect on the data was confirmed by the data from Ansys. A filter was applied so that all the input parameters were constant except the nanoparticle diameter. The outcome of the Nusselt number

and pressure drop was almost the same for all four nanoparticle diameters. The Nusselt number did have a variation; however, this was so small that it could be neglected.

It is evident from Table 7 that the lower nanoparticle diameter resulted in a higher pressure drop. This was due to the higher velocity in the channels for the smaller nanoparticle diameter. The higher Nusselt number for the smaller nanoparticles was related to the added Brownian motion relative surface area. The larger surface area of the smaller nanoparticles enhanced the heat transfer and allowed for a larger Nusselt number. However, the change in the Nusselt number is so small that this cannot be confirmed, thus enforcing the conclusion that the diameter has little to no effect on the heat transfer characteristics and pressure drop in case studies. The fluid flow rate and the fluid velocity of Al_2O_3-water nanofluid are listed in Table 8 to demonstrate the higher pressure drop of the smaller diameter. The higher pressure drop was due to the viscosity increase with smaller diameter because the diameter was in the denominator of the viscosity equation.

In conclusion, the effect of the diameter on the system was extremely small; however, there was some evidence when altering the data for the flow rate and velocity. The lower the diameter, the larger the specific heat removal area, inducing a larger pressure drop and a larger Nusselt number. However, the optimal result could not be concluded because some specific region between the diameters could exist where the Nusselt number was high while the pressure drop was lower. This was another indication that an optimisation was needed for more clarification. Figures 18 and 19 show the effect of the nanoparticle diameters on the Nusselt number and the pressure drop of Al_2O_3-water, CuO-water, SiO_2-water and ZnO-water nanofluids. The same trend can be seen as in Table 7 where the influence of the nanoparticle diameters on the outcome was small.

REGRESSION MODEL OF THE NUMERICAL RESULTS

Outputs and corresponding inputs of numerical simulation in Ansys Fluent were exported into Microsoft Excel and MATLAB for further analysis. This highlighted some functions and relations between the inputs and outputs to correctly design further optimisation. The optimisation algorithm works in two steps of performing regression on the prepared data and optimising the regression functions. In these two steps, the regression model proposes two functions, one function for the Nusselt number and one for the pressure drop. The two functions are then later used to maximise the Nusselt number function and minimise the pressure drop function. The chosen method for regression was the radial basis function (RBF). The power of RBF lies in the radial format so that it can be used in more than one dimension. This method is a good choice when users have gone to great lengths of ensuring that the data is precise in order not to lose accuracy with the addition of a function that only approximates the data. RBF functions go perfectly through each of the given data points.

A radial basis function is translation of a radially symmetric function that is linearly combined to approximate an unknown function, so that the following can be stated:

$$\varphi(X) = \varphi(\|X\|) \tag{18}$$

Any function that satisfies Equation (18) can be classified as a radial function. The computing of an RBF uses in most parts the reconstruction of an unknown function for known data. This also satisfied the data format of the current study where the known data came from Ansys Fluent having known inputs and outputs. An RBF can be used as a collection $\{\varphi_k\}_k$, which then forms a function of interest. Approximates of functions are done by summation of the radial base function at each data point. The general form for a radial basis function can be seen in Equation (19):

$$s(x) = \{\sum\nolimits_{\zeta \epsilon \Xi} \lambda_\zeta \|\cdot - \zeta\| | \lambda_\zeta \in R\} \tag{19}$$

where ζ refers to the data sites, λ_ζ is the real coefficients and $\|\quad\|$is the Euclidean distance from the origin. In Equation (19), the radial basis function is simply described as $\varphi(r_r) = r_r$.

Each data set can be different. For the model to be universal with any nanofluid and any iteration of the designed inputs, an in-house code was written, which tested each different radial basis function and determined the best-fitting one. Most RBF functions also include the use of a shape factor influencing the scale of the input to better fit the data.

Shape factors are difficult to determine because they are heavily influenced by the specific data set. Most shape factors are determined by trial and error. However, as the model must determine the shape factor for each new data set given, the shape factor will be determined once for the data set using another script. This script will change the shape factor and determine the goodness of fit from the error of the output from the function for a given input. To ensure universal implementation of the model, the different equations in Table 9 were all implemented with the RBF function and the error calculated. This would determine the optimal RBF function for each data set independently. Optimal RBF function ensured that any new data generated by the numerical simulations could still be optimised. This also added value to the model to ensure further use without alterations being needed.

Error behaviour in radial basis functions are local and are in terms of the distance from the centre discrete variables. For some of the infinitely smooth RBF's, the interpolation error converges at an exponential rate; for instance, Gaussian and inversely multiqaudric. The distance to the centres can be calculated from the following equation:

$$h_h \coloneqq h_h(X, \Omega) \coloneqq min\|x - y\| \tag{20}$$

by using the discrete set of centres X in respect of the chosen working domain Ω.

One of the reasons for choosing RBF is the curse of dimensionality and the ability of RBF to overcome this obstacle. The curse of dimensionality was also seen in this project, where four inputs and one output were present with the output being either the Nusselt number or the pressure drop and the inputs being the nanoparticle volumetric concentration, nanoparticle diameter, base fluid and nanoparticle type. The only way to show this equation and the effect of the implemented RBF on the data was by showing a 3D case of the data. Both cases showed how an RBF would look on the data if less inputs were chosen. The implemented RBFs are shown in Figures 20 and 21. However, it was not possible to demonstrate how it would look because a 5D solution could not be represented visually.

MULTI-OBJECTIVE OPTIMISATION MODEL BASED ON THE NUMERICAL RESULTS

An in-house multi-objective optimisation code was used to do the optimisation. The concept was that the Nusselt number had to be maximised, and the pressure drop minimised at the same time to determine the combination of inputs that had the best heat transfer for the lowest pressure drop. The algorithm used was a modified NSGA. This algorithm would not only give one optimal solution but a Pareto optimal solution, which is a front of solutions each showing an optimal point for the system. In the past, NSGA was criticised for large computational complexity, no elitism in the approach, and calculation of sharing parameter [27, 28]. These problems were fixed in a new method proposed by Deb et al. [29]. This new method was adopted and used for the in-house code. The modified NSGA consists of different operators that work together to create a robust technique. The fast non-dominating sorting operator, crowding distance operator and their connections are described in the authors' previous work of [30]. The solution to the three suggested problems listed above was as follows:

1) The computational complexity was reduced from $O(MN^3)$ to $O(MN^2)$ by calculating a domination count with each front. After each front was calculated, the domination count was lowered and the front was stored in another list, this process continued for each front. Therefore, the domination count could at most be N-1, ensuring that each solution was only visited N-1 times.
2) Elitism was introduced by comparing the current front with previously optimal solutions.
3) The sharing function was replaced with a crowded-comparison approach. A density estimation technique was added to determine the exact state of the diversity in the system. The overall crowding factor was calculated by the summation of individual distances to each objective. This was then used as a crowded comparison operator calculated at each front, which drove the selection process to diversify.

Both objectives were specified, and the number of input parameters was given. The code offered a selection of the number of generations and the number of populations. These inputs differed from simulation to simulation as well as data specifics. Generations were used as children mutated from the parents, where the population showed the number of different entries that were tried and tested for each generation. It was seen through some trial and error that a generation count of 200 and a population count of 2 000 offered the best results. This was because the data set was densely packed and large variation was not needed. However, the densely packed data needed precision because the values were small and close to one another.

As stated previously, the Pareto front is generated with the modified NSGA algorithm giving multiple answers and ensuring the user can choose a selection that will practically and experimentally work. The outcome of the algorithm was added back into Ansys to ensure that the generated Nusselt number and pressure drop were still correct, and the RBF functions and modified

NSGA were validated in this way. The results showed that SiO_2-water nanofluid with concentration of 0.01 regardless of the nanoparticle diameter was the best-performing nanofluid.

CONCLUSIONS

The study set out to model and optimise nanofluids in microchannels to achieve the highest heat transfer rate and the lowest pressure drop. This was done by gaining knowledge on the theory of fluid flow in microchannels and the material behaviour models used to characterise these nanoparticles in a fluid. The geometry was selected to be a small microchannel that would fit onto a computer chip. The models of material property selection defining the behaviour of nanofluids were selected to have enough parameters that could be changed for later optimisation. The results of the numerical simulation were validated with numerical and experimental work. This simulation was duplicated to ensure the flow regime would stay the same, while the material properties were changed in relation to the different inputs. The inputs that were changed were the base fluid, nanoparticle type, volumetric concentration of nanoparticles and nanoparticle diameter. A data set of 256 different combinations of these inputs was created to have enough data points for simulation. Four of each of the inputs were chosen to create the different combinations. A model was created that would make this data set all automatic so that the user could change the input bounds and thus simulate other particle types, diameters, volumetric concentrations, or base fluids, if new data was needed. This allows the user to enter his or her own inputs into any of the selected parameters and test the usefulness of these new inputs to the current data.

The data set was then characterised by RBF to precisely go through all the points. Two functions were created to supply the genetic algorithm with two objective functions, one to be maximised (Nusselt number) and one to be minimised (pressure drop). This would yield an optimal answer

where the heat transfer and pumping efficiency were maximised. This algorithm was run through the generated Ansys data and the outcome of the present research work was a success. The optimal point was then added into Ansys Fluent again for verification and validation to ensure that the RBF and the modified NSGA were accurate. There was a 1-3% error in the results and this was due to rounding errors made in the transfer from Ansys Workbench to MATLAB.

ACKNOWLEDGEMENTS

The support and resources of South African CSIR/DST Centre for High Performance Computing (CHPC) are gratefully acknowledged.

NOMENCLATURE

C_p Specific heat capacity ($\frac{J}{kg.K}$)

C_μ Empirical coefficient of eddy viscosity

$C_{1\varepsilon}$ Dissipation rate constant

$C_{2\varepsilon}$ Dissipation rate constant

D_h Hydraulic diameter (m)

d_{np} Diameter of nanoparticle (m)

E_{ij} Rate of deformation ($\frac{1}{s}$)

F Pressure drop coefficient

f_1 First-finest grid solution

f_2 Second-finest grid solution

F_s Safety factor

GCI Grid convergence index

h Heat transfer coefficient ($\frac{W}{m^2.K}$)

h_h Distance to centres

k Thermal conductivity ($\frac{W}{m.K}$)

k Turbulence kinetic energy ($\frac{m^2}{s^2}$)

K_B Boltzmann constant ($\frac{J}{K}$)

k_{eff} Effective thermal conductivity of nanofluid ($\frac{W}{m.K}$)

NSGA Non-dominated sorting genetic algorithm

Nu Nusselt number

p Pressure (Pa)

q_w Heat flux at base plate ($\frac{W}{m^2}$)

Q Fluid volumetric flow rate ($\frac{m^3}{s}$)

RBF Radial basis function

Re Reynolds number

r Mesh refinement ratio

r_r Radius

s Radial basis function general form

T Temperature (K)

t Time (s)

u Velocity ($\frac{m}{s}$)

u_i Velocity component in the corresponding direction ($\frac{m}{s}$)

UDF User-defined function

V Velocity ($\frac{m}{s}$)

y^+ Dimensionless wall distance

X Discrete set of centres

x, y, z Coordinate system

Greek symbols

β Empirical parameter that represents the hydrodynamic interaction between particles and affected fluid

ρ Density ($\frac{kg}{m^3}$)

ϕ Nanofluid volumetric concentration

μ Dynamic viscosity ($\frac{N.s}{m^2}$)

μ_t Eddy viscosity ($\frac{N.s}{m^2}$)

σ_k Prandtl number for turbulent kinetic energy

σ_ε Prandtl number for turbulent kinetic energy dissipation rate

ε Turbulent kinetic energy dissipation rate ($\frac{m^2}{s^3}$)

ζ Data sites

λ_ζ Radial basis function coefficients

φ Radial basis function

Ω Working domain

Subscripts

ave Average

b Bulk

f Base fluid

hs Heat sink

np Nanoparticle

nf Nanofluid

o Initial

s Solid

w wall

Superscripts

pp Order of convergence

REFERENCES

[1] S. U. S. Choi, J.A. Eastman, “Enhancing thermal conductivity of fluids with nanoparticles,” presented at the 1995 ASME International Mechanical Engineering Congress and Exposition (IMECE1995), San Francisco, CA, USA, November 12-17, 1995.

[2] S. U. S. Choi, Z. G. Zhang, W. Yu, F. E. Lockwood, and E. A. Grulke, “Anomalous thermal conductivity enhancement in nanotube suspensions,” *Appl. Phys. Lett*., vol. 79, no. 14, pp. 2252-2254, August 2001. DOI: 10. 1063/1.1408272.

[3] F. Yuan, J. Lin, and X. Ku, “Convective heat transfer and resistance characteristics of nanofluids with cylindrical particles,” *Heat Transf. Eng*., vol. 39, no. 6, pp. 526-535, 2018. DOI: 10.1080/01457632.2017.1320166.

[4] D. B. Tuckerman and R. Pease, “High-performance heat sinking for VLSI,” *IEEE Electron Device Lett.*, vol. 2, no. 5, pp. 126-129, May 1981. DOI:10.1109/EDL.1981.25367.

[5] J.L. Xue, Y.H. Gan, D.C. Zhang, and X.H. Li, “Microscale heat transfer enhancement using thermal boundary layer redeveloping concept,” *Int. J. Heat Mass Transf*., vol. 48, no. 9, pp. 1662-1674, April 2005. DOI:10.1016/j.ijheatmasstransfer.2004.12.008.

[6] P.-S. Lee, S.V. Garimella, and D. Liu, “Investigation of heat transfer in rectangular microchannels,” *Int. J. Heat Mass Transf*., vol. 48, no. 9, pp. 1688-1704, April 2005. DOI:10.1016/j.ijheatmasstransfer.2004.11.019.

[7] A. J. L. Foong, N. Ramesh, and T. T. Chandratilleke, “Laminar convective heat transfer in a microchannel with internal longitudinal fins,” *Int. J. Therm. Sci*., vol. 48, no. 10, pp. 1908-1913, October 2009. DOI:10.1016/j.ijthermalsci.2009.02.015.

[8] R. Prasher, D. Song, J. Wang, and P. Phelan, “Measurements of nanofluid viscosity and its implications for thermal applications,” *Appl. Phys. Lett.*, vol. 89, no. 13, pp. 133103-133108, July 2006. DOI: 10.1063/1.2356113.

[9] Y. Xuan, Q. Li, and W. Hu, “Aggregation structure and thermal conductivity of nanofluids,” *AIChE J.*, vol. 49, no. 4, pp. 1038-1043, April 2003. DOI: 10.1002/aic.690490420.

[10] K. B. Anoop, T. Sundararajan, and S. K. Das, “Effect of particle size on the convective heat transfer in nanofluid in the developing region,” *Int. J. Heat Mass Transfer*, vol. 52, no. 9-10, pp. 2189-2195, April 2009. DOI: 10.1016/j.ijheatmasstransfer.2007.11.063.

[11] M. Kahani. “Simulation of nanofluid flow through rectangular microchannel by modified thermal dispersion model,” *Heat Transf. Eng*, vol. 41, no. 4, pp. 377-392, January 2020. DOI: 10.1080/01457632.2018.1540464.

[12] T. Coşkun and E. Çetkin, “Heat transfer enhancement in a microchannel heat sink: nanofluids and/or micro pin fins,” *Heat Transf. Eng.*, vol. 41, no. 21, 2020 (in press). DOI: 10.1080/01457632.2019.1670467.

[13] A. Abdollahi, R. N. Sharma, H.A. Mohammed & A. Vatani, “Heat transfer and flow analysis of Al_2O_3-Water nanofluids in interrupted microchannel heat sink with ellipse and diamond ribs in the transverse microchambers,” *Heat Transf. Eng.*, vol. 39, no. 16, pp. 1461-1469, 2018. DOI: 10.1080/01457632.2017.1379344.

[14] L. M. Tam, A. J. Ghajar, and H. K. Tam, “Contribution analysis of dimensionless variables for laminar and turbulent flow convection heat transfer in a horizontal tube using artificial neural network,” *Heat Transf. Eng.*, vol. 29, no. 9, pp. 793-804, 2008. DOI: 10.1080/01457630802053827.

[15] M. Mehrabi, S.M.A Noori Rahim Abadi, and J.P. Meyer, “Heat transfer and fluid flow optimization of titanium dioxide-water nanofluids in a turbulent flow regime,” *Heat Transf. Eng.*, vol. 41, no. 1, pp. 36-49, January 2020. DOI: 10.1080/01457632.2018.1513623.

[16] R. Chein and J. Chen, “Numerical study of the inlet/outlet arrangement effect on microchannel heat sink performance,” *Int. J. Therm. Sci.*, vol. 48, no. 8, pp. 1627-1638, August 2009. DOI: 10.1016/j.ijthermalsci.2008.12.019.

[17] A. Abdollahi, H. A. Mohammed, S. M. Vanaki, A. Osia, and M. R. Golbahar Haghighi, “Fluid flow and heat transfer of nanofluids in microchannel heat sink with V-type inlet/outlet arrangement,” *Alexandria Eng. J.*, vol. 56, no. 1, pp. 161-170, February 2017. DOI: 10.1016/j.aej.2016.09.019.

[18] Ansys, I. ‘Ansys Fluent Theory Guide’, *ANSYS Inc., Canonsburg, PA, USA*, 15317 (November), pp. 724-746, 2013.

[19] P.J. Roache, "Perspective: a method for uniform reporting of grid refinement studies," *ASME.* J. Fluids Eng., vol. 116, no. 3, pp. 405-413, September 1994, DOI: 10.1115/1.2910291.

[20] Chpc.ac.za., *Centre for high performance computing*. [online] Available at: https://www.chpc.ac.za/ [Accessed 5 Feb. 2020].

[21] R. J. Philips, “Micro-Channel Heat Sinks,” in *Advances in Thermal Modeling of Electronic Components and System*, A. Bar-Cohen and A. D. Kraus, Eds. New York, USA: ASME, 1990.

[22] J. Koo, and C. Kleinstreurer, “Viscous dissipation effects in microtubes and microchannels”, *Int. J. Heat Mass Transf.*, vol. 47, no. 14-16, pp. 3159-3169, July 2004. DOI: 10.1016/j.ijheatmasstransfer.2004.02.017.

[23] J.C. Maxwell and J.J. Thompson, *A Treatise on Electricity and Magnetism*, Oxford, UK: Clarendon Press, 1873.

[24] H. A. Mohammed, P. Gunnasegaran, and N. H. Shuaib, “Heat transfer in rectangular microchannels heat sink using nanofluids,” *Int. Commun. Heat Mass Transf.*, vol. 37, pp. 1496-1503, December 2010. DOI:10.1016/j.icheatmasstransfer.2010.08.020.

[25] CES EduPack, Cambridge, UK: Granta Design Limited, 2009.

[26] American Society of Heating, Refrigerating and Air-Conditioning Engineers, *2017 ASHRAE handbook. Fundamentals*. Atlanta, GA, USA: ASHRAE, 2017.

[27] E. Zitzler, K. Deb, and L. Thiele, “Comparison of multi objective evolutionary algorithms: empirical results” *Evol. Comput.*, vol. 8, no.2, pp. 173-195, 2000. DOI: 10.1162/106365600568202.

[28] Fonseca, C. M. and Fleming, P. J. (1998) “Multi objective optimization and multiple constraint handling with evolutionary algorithms - Part I: A unified formulation,” *IEEE Trans. Syst., Man, Cybern. A, Syst. Humans.*, vol. 28, no. 1, pp. 26-37, January 1998. DOI: 10.1109/3468.650319.

[29] K. Deb, A. Pratap, S. Agarwal, and T. Meyarivan, “A fast and elitist multi objective genetic algorithm: NSGA-II,” *IEEE Trans. Evol. Comput*., vol. 6, no. 2, pp. 182-197, August 2002. DOI: 10.1109/4235.996017.

[30] S. N. R. Abadi, M. Mehrabi, and J. P. Meyer, "Prediction and optimization of condensation heat transfer coefficients and pressure drops of R134a inside an inclined smooth tube," *Int. J. Heat*

Mass Transf., vol. 124, pp. 953-966, September 2018. DOI: 10.1016/j.ijheatmasstransfer.2018.04.027.

Table 1. GCI mesh independence

Design point	Mesh density	GCI
1	100 000	
2	150 000	0.767
3	250 000	0.864
4	350 000	0.923
5	500 000	0.976
6	1 000 000	0.9998

Table 2. Comparison between the errors of Chein and Chen [16] and Abdollahi et al. [17] and the present study in each channel of the microchannel

Error %	1	2	3	4	5	6	7	8	9	10	11
[16]	0.693	1.329	0.561	0.978	0.673	0.557	0.500	0.645	0.673	0.450	1.538
[17]	1.284	1.329	0.306	0.264	0.522	0.451	0.429	0.663	0.779	0.450	1.538

Table 3. Inputs of the present study for base fluids, nanoparticles, volumetric concentration, and nanoparticle diameters

Inputs	Base fluid	Nanoparticle	Volumetric concentration	Diameter (nm)
1	Water	Al_2O_3	0.001	10
2	Ethylene glycol	CuO	0.005	30
3	W/EG 50/50	SiO_2	0.01	60
4	W/EG 60/40	ZnO	0.05	100

Table 4. Thermophysical properties of the nanoparticles [17]

Thermophysical properties	Al_2O_3	CuO	SiO_2	ZnO
$\rho(\frac{kg}{m^3})$	3970	6500	2200	5600
$C_p(\frac{J}{kg\ K})$	765	535.6	703	495.5
$k(\frac{W}{m\ K})$	40	20	1.2	13

Table 5. Thermophysical properties of the base fluids [26]

Thermophysical properties	Water	Ethylene glycol	W/EG 50/50	W/EG 60/40
$\rho(\frac{kg}{m^3})$	998.2	1113.2	1055.7	1044.2
$C_p(\frac{J}{kg\ K})$	4182	2360	3221.38	3405
$k(\frac{W}{m\ K})$	0.609	0.258	0.429	0.463
$\mu(\frac{Ns}{m^2})$	0.001002	0.0161	0.0085515	0.0078418

Table 6. Ansys Workbench input for Al_2O_3-water nanofluids with particle diameters of 10 nm

Design point	Density (kg/m^3)	C_P (J/kg. K)	Viscosity ($N.s/m^2$)	Thermal conductivity (W/m. K)	Volumetric concentration
1	1001.2	4168.5	0.001	0.601	0.001
2	1013.1	4115	0.001	0.603	0.005
3	1028	4050	0.001	0.606	0.01
4	1146.8	3591.5	0.001	0.627	0.05

Table 7. Effect of the nanoparticle diameter on the Nusselt number and pressure drop of Al_2O_3-water nanofluid when the volumetric concentration is 0.01

Design point	Diameter (nm)	Nusselt number	Pressure drop (Pa)
1	10	26.8	65106
2	30	26.4	63887
3	60	26.4	63887
4	100	26.4	63887

Table 8. Effect of the nanoparticle diameter on the velocity and flow rate of Al_2O_3-water nanofluid when the volumetric concentration is 0.01

Design point	Diameter (nm)	Velocity (m/s)	Flow rate (m^3/s)
1	10	5.9	4.41×10^{-6}
2	30	5.9	4.32×10^{-6}
3	60	5.6	4.16×10^{-6}
4	100	5.5	4.15×10^{-6}

Table 9. Radial basis functions used to approximate the data in this study

RBF	$\varphi(r_r)$
Linear	εr_r
Cubic	$(\varepsilon r_r)^3$
Thin plate	$(\varepsilon r_r)^2 \log(\varepsilon r_r)$
Quadratic	$1 + (\varepsilon r_r)^2$
Multiquadric	$\sqrt{1 + (\varepsilon r_r)^2}$
Inverse multiquadric	$\frac{1}{\sqrt{1 + (\varepsilon r_r)^2}}$
Inverse quadric	$\frac{1}{1 + (\varepsilon r_r)^2}$
Gauss	$e^{-(\varepsilon r_r)^2}$

List of Figures

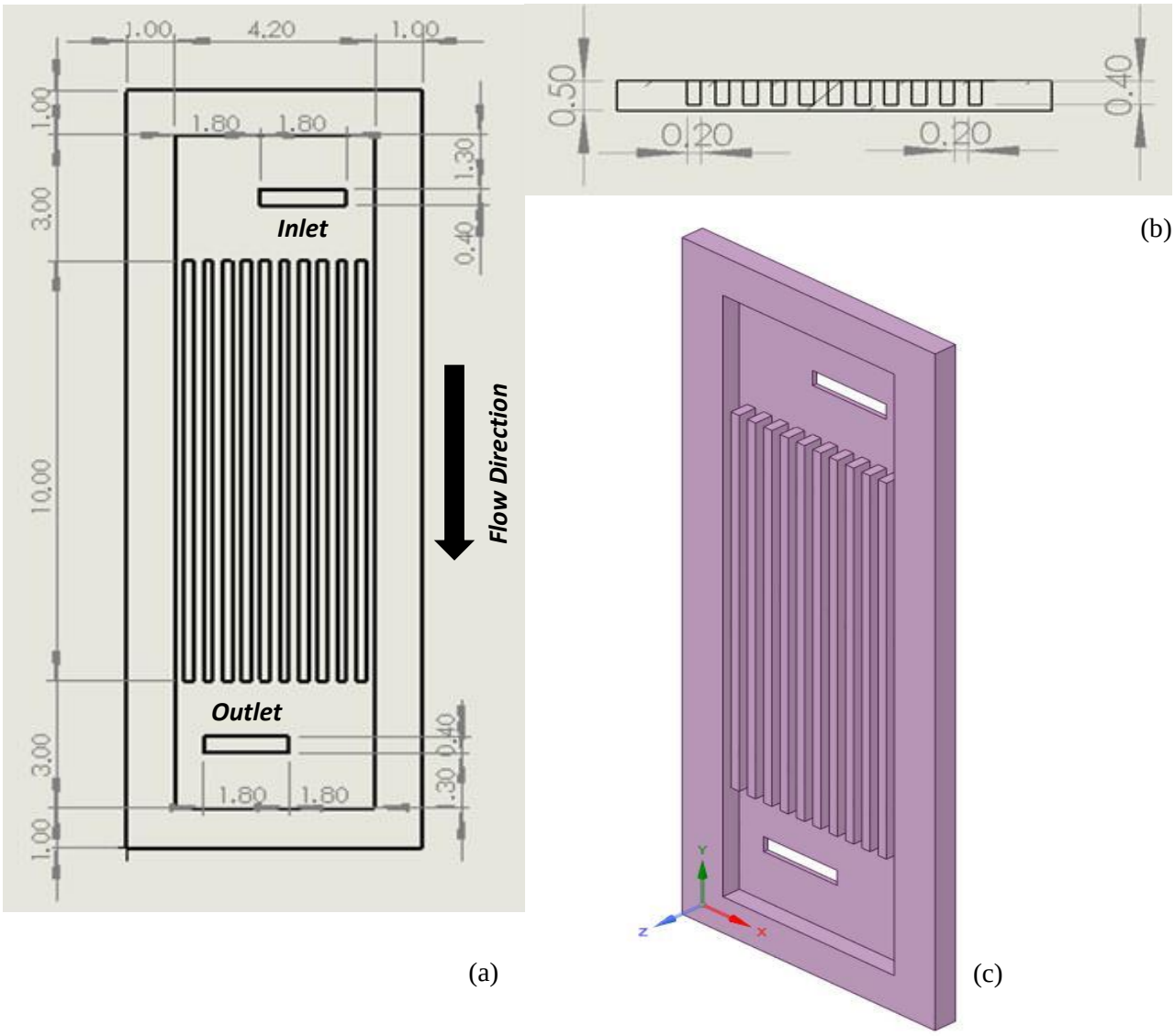

Figure 1. Microchannel geometry in mm: (a) front view of the microchannel, (b) top view of the microchannel and (c) 3D view of the microchannel.

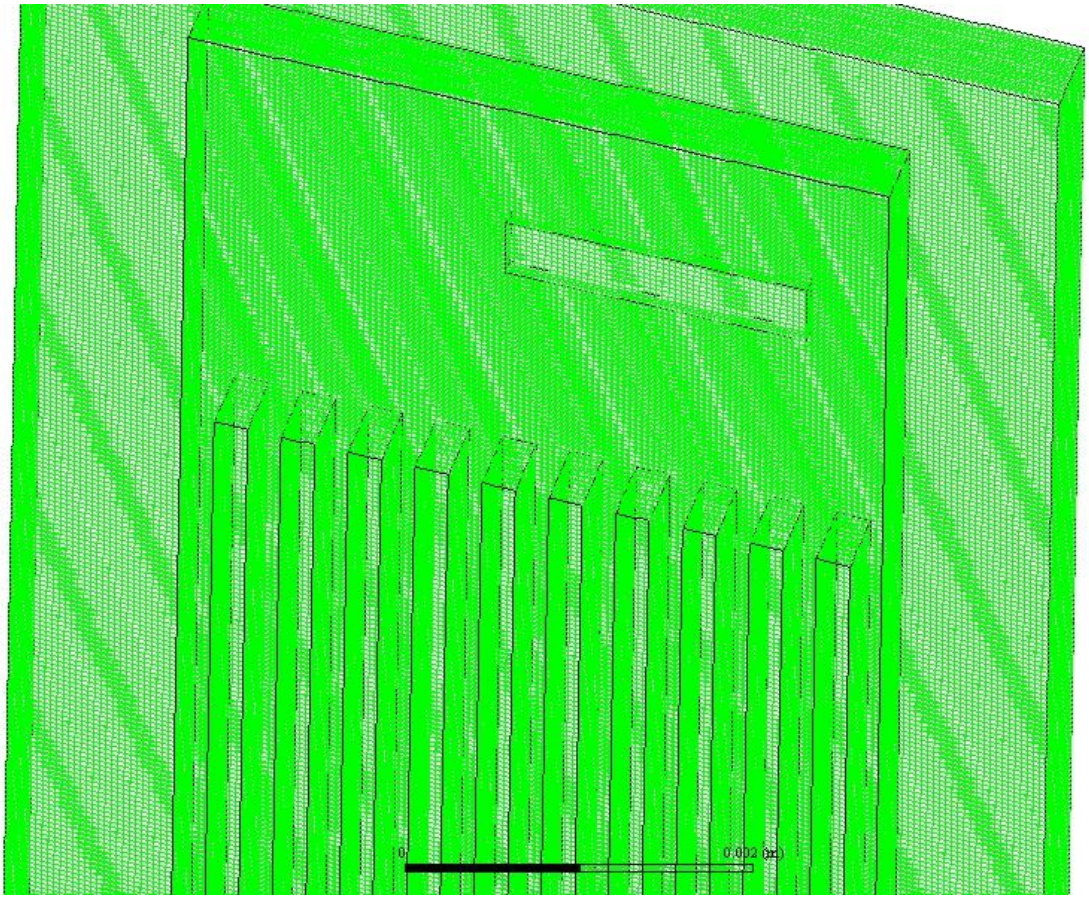

Figure 2. 3D section mesh display of the microchannel.

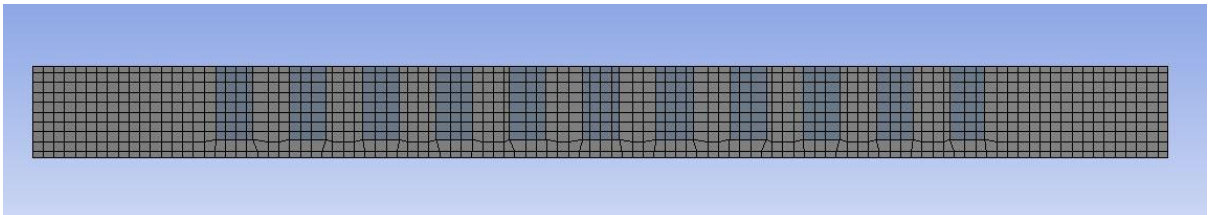

Figure 3. Section plane mesh display of the microchannel.

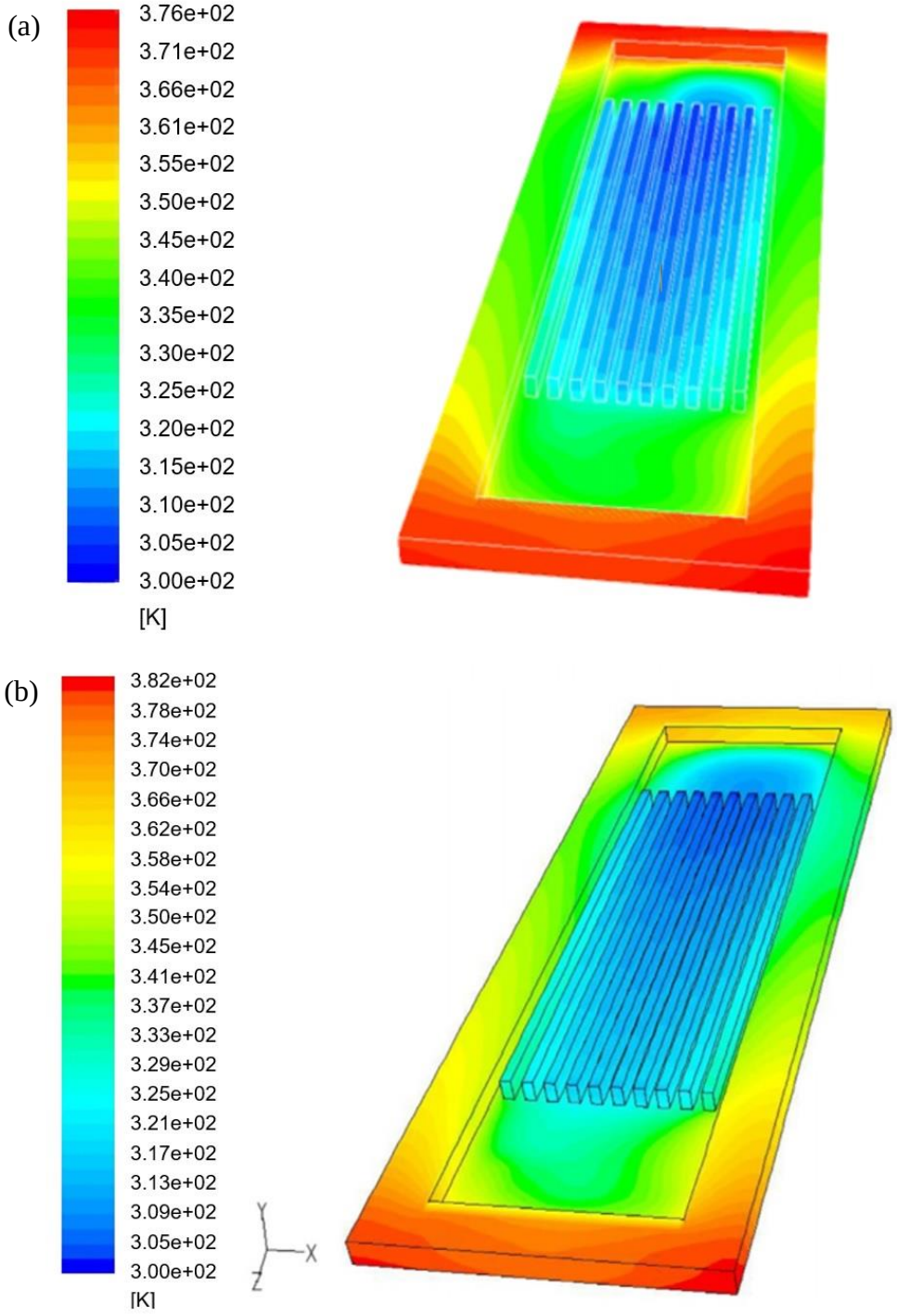

Figure 4. (a) Numerical results of Chein and Chen [16], (b) numerical results of Abdollahi et al. [17].

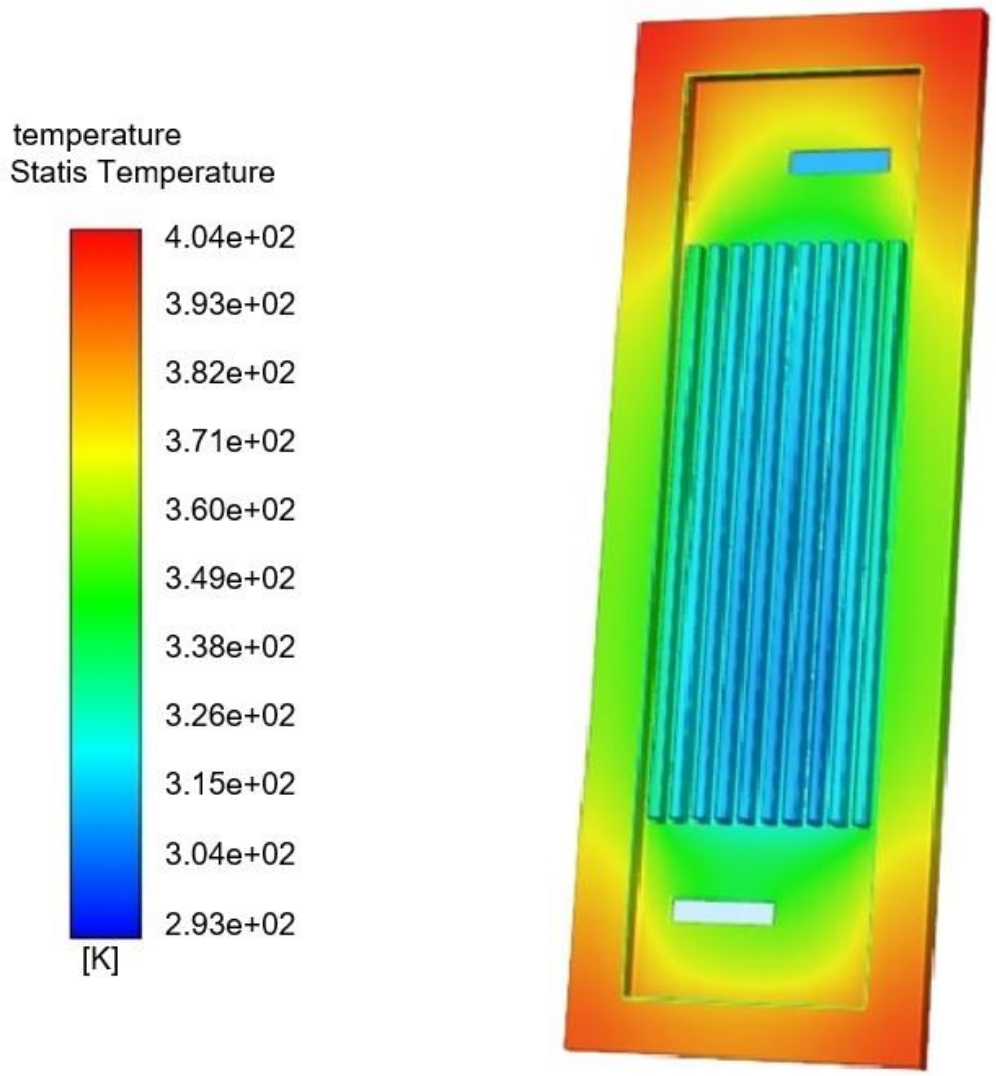

Figure 5. Numerical results of the present work: mid-section plane of the temperature contour.

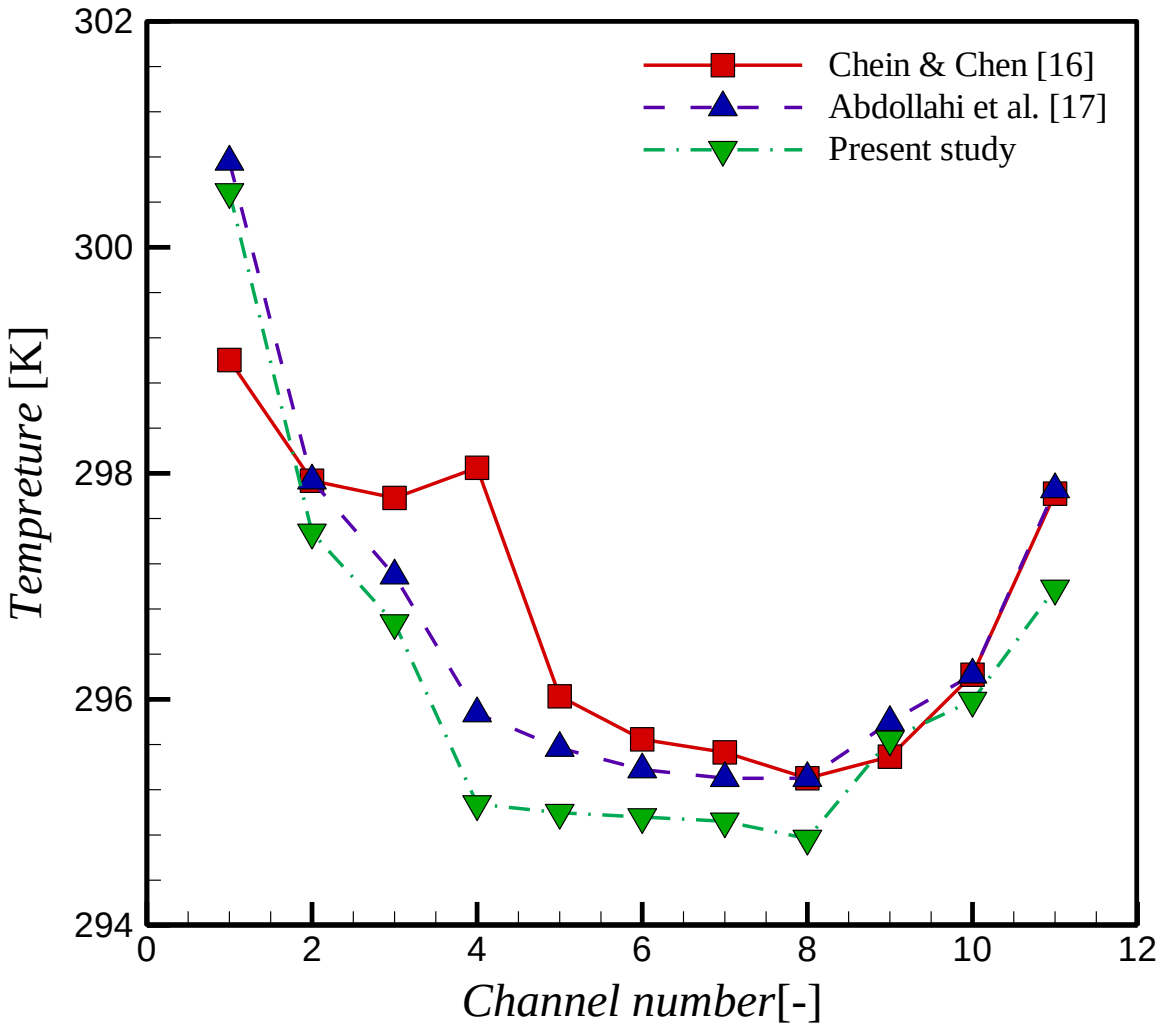

Figure 6. Comparison between the results of Chein and Chen [16], Abdollahi et al. [17] and the present study for the average temperature of water in different channels of the microchannel.

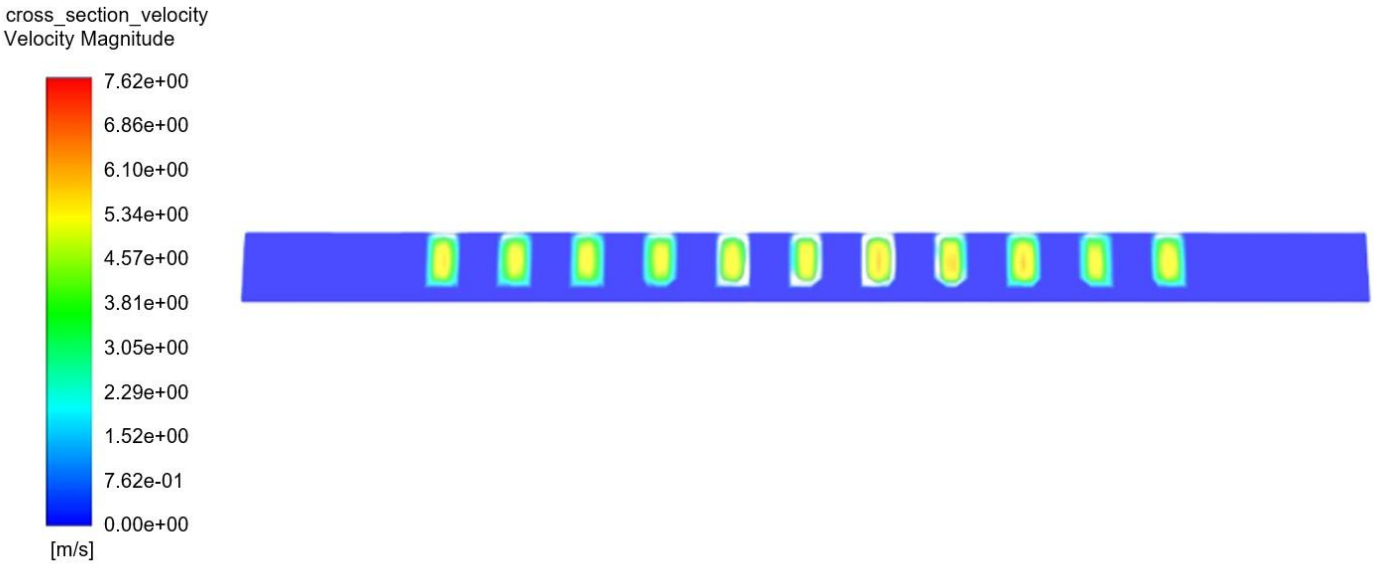

Figure 7. Numerical results of the present work: cross-section of the velocity contour.

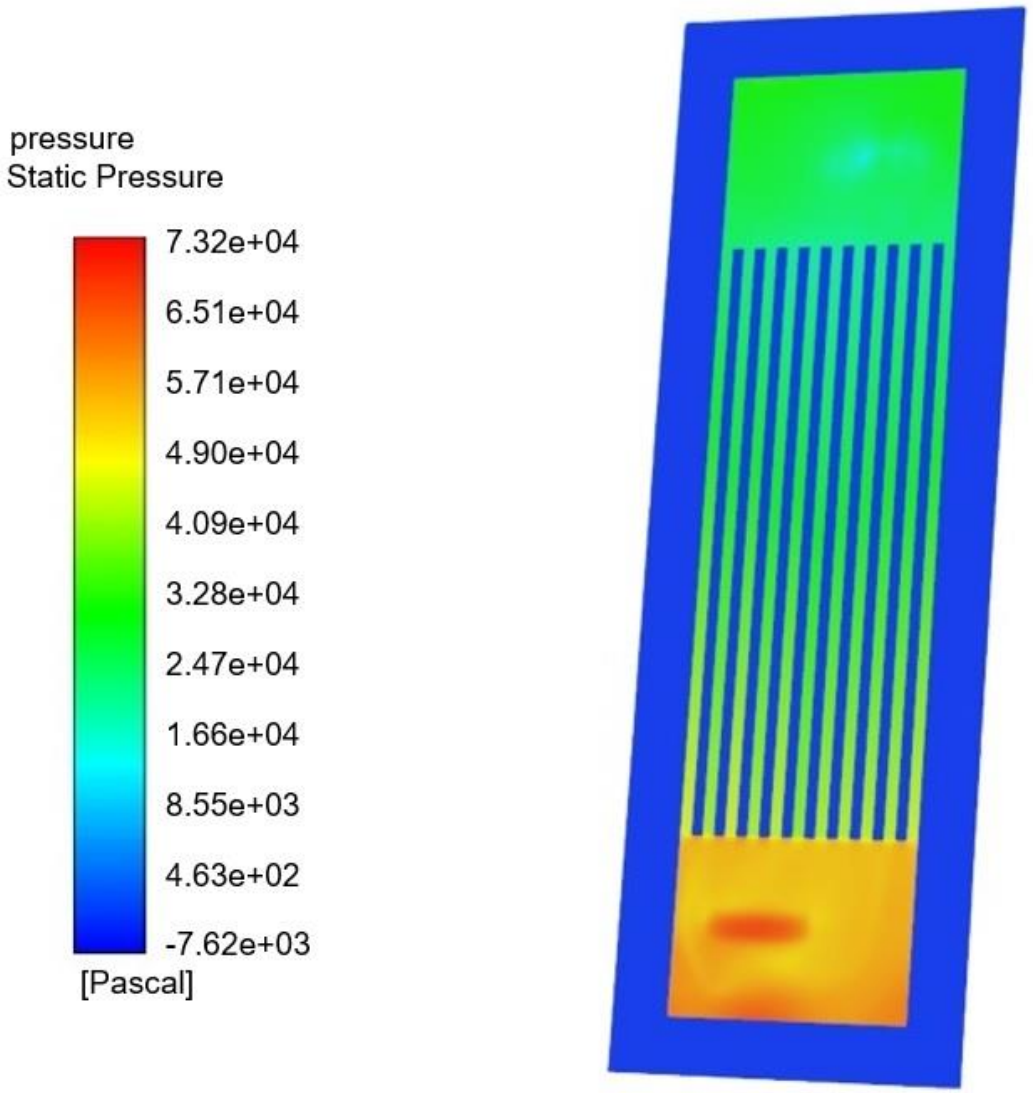

Figure 8. Numerical results of the present work: mid-section plane of the pressure contour.

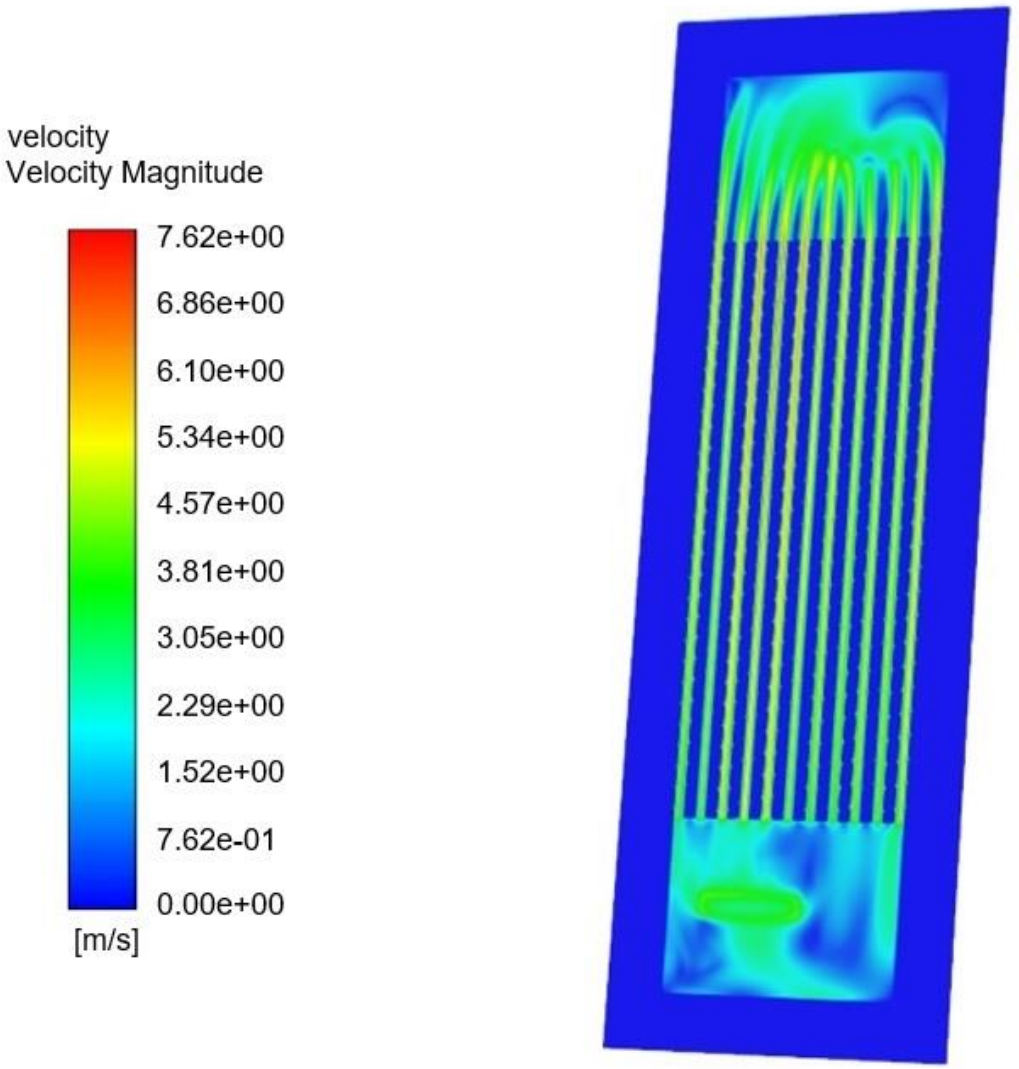

Figure 9. Numerical results of the present work: mid-section plane of the velocity contour.

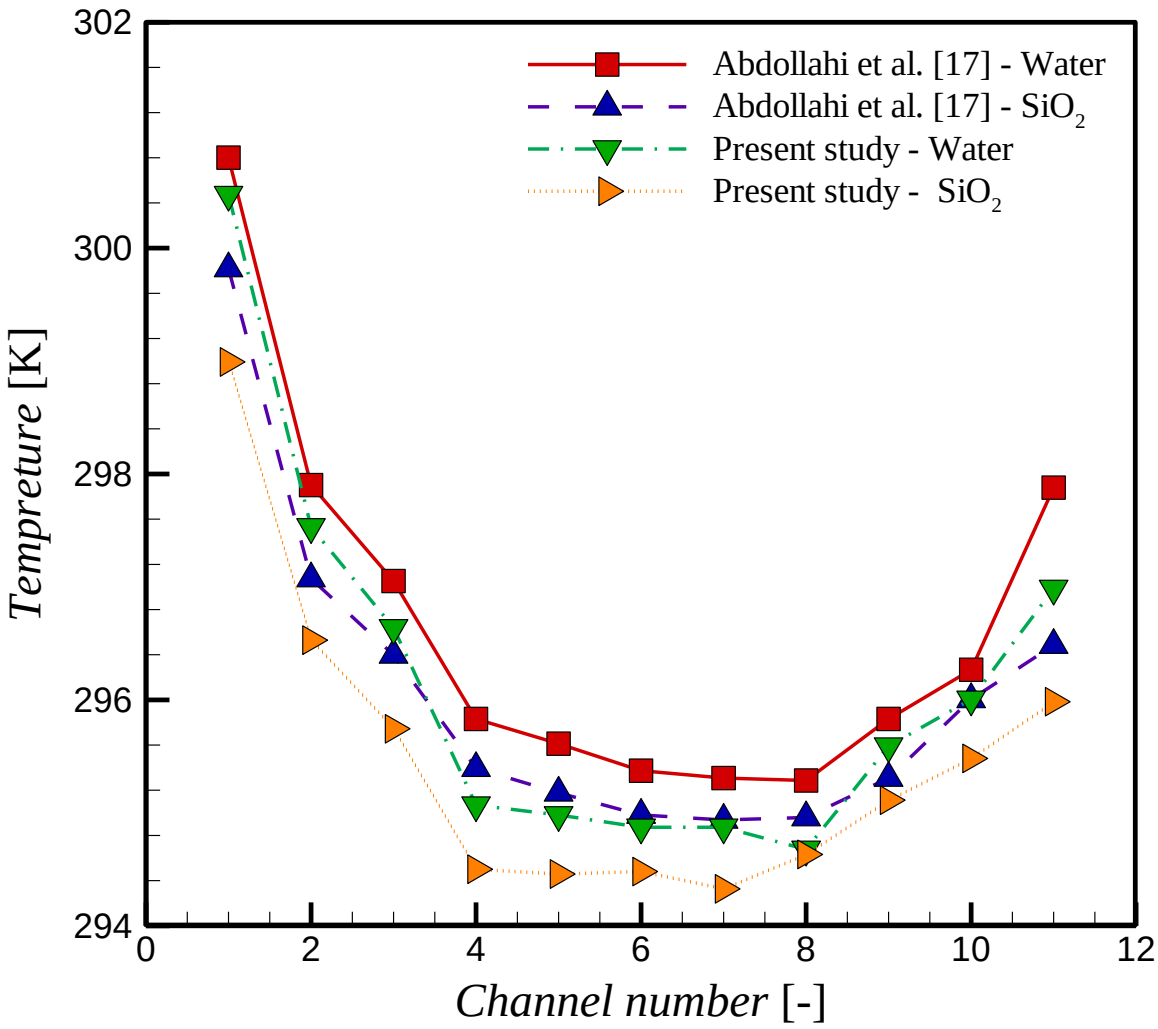

Figure 10. Comparison between the results of Abdollahi et al. [17] and the present work for the average temperatures of water and nanofluid (SiO_2) in different channels of the microchannel.

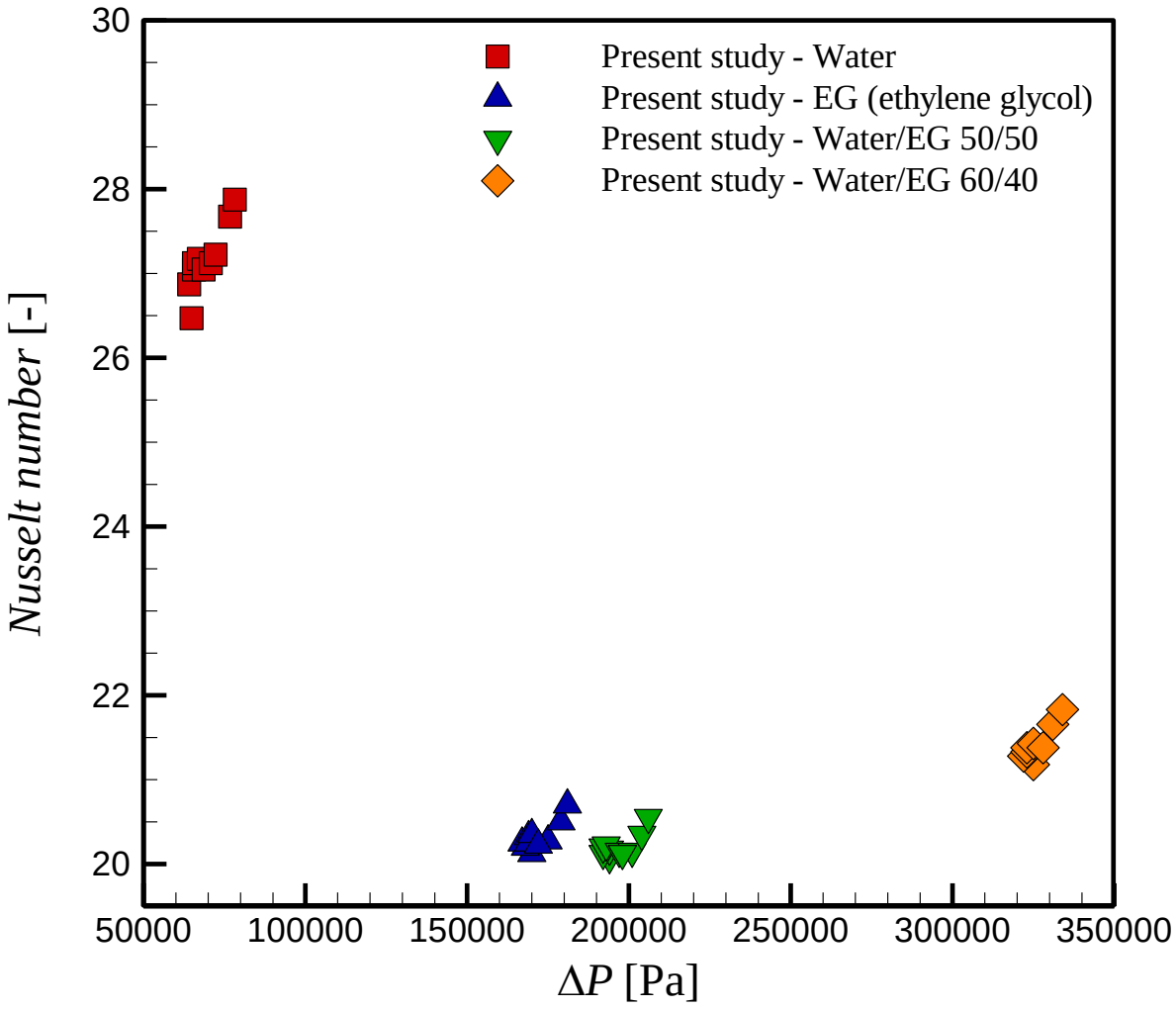

Figure 11. Effect of base fluids on the Nusselt number and pressure drop of nanofluids for four different base fluids and various volumetric concentration and nanoparticle diameters.

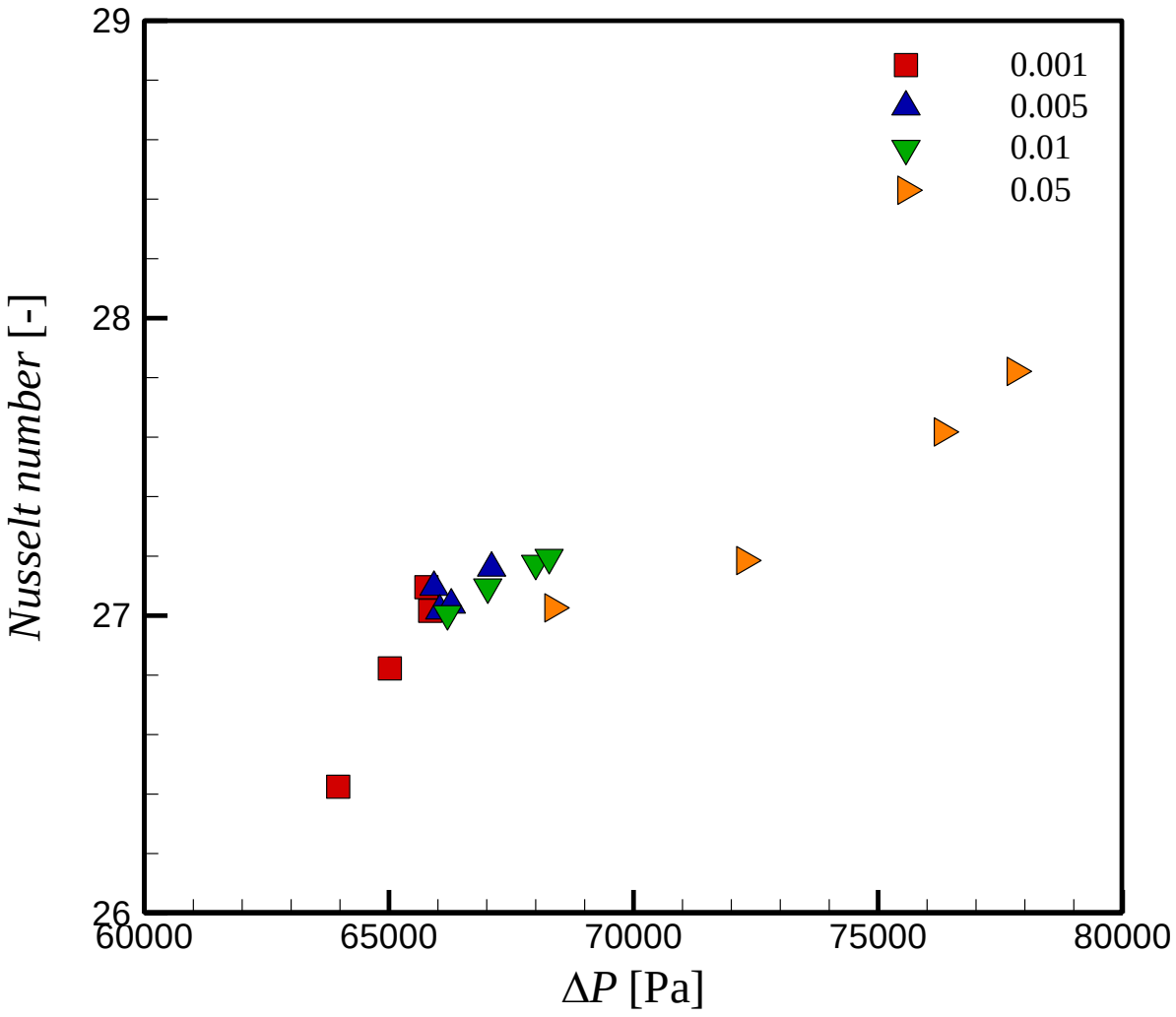

Figure 12. Effect of nanoparticle volumetric concentration on the Nusselt number and pressure drop of nanofluids for four different base fluids and various volumetric concentration and nanoparticle diameters.

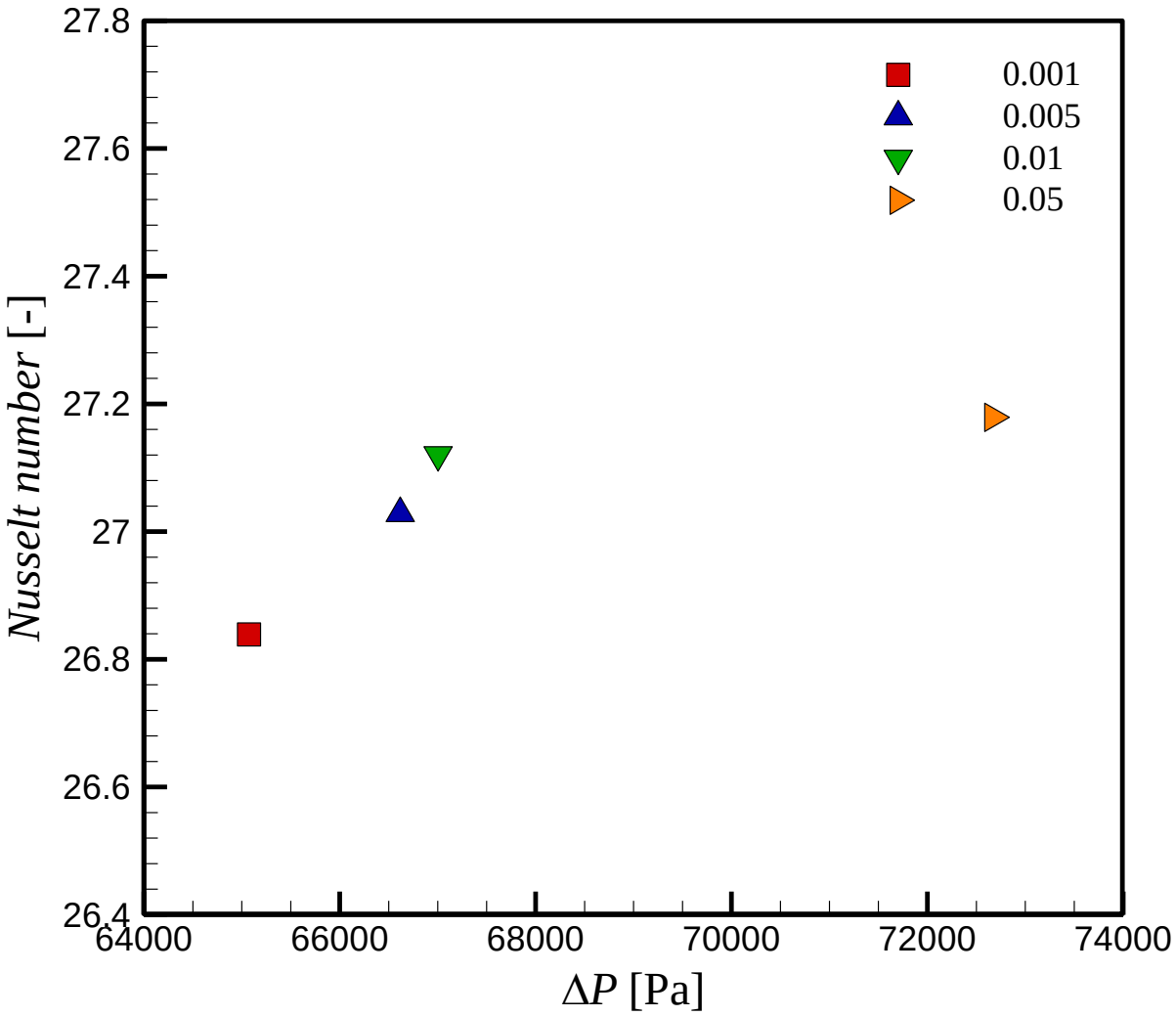

Figure 13. Effect of the nanoparticle volumetric concentration on the Nusselt number and pressure drop of SiO_2-water nanofluid when the nanoparticle diameter is 100 nm.

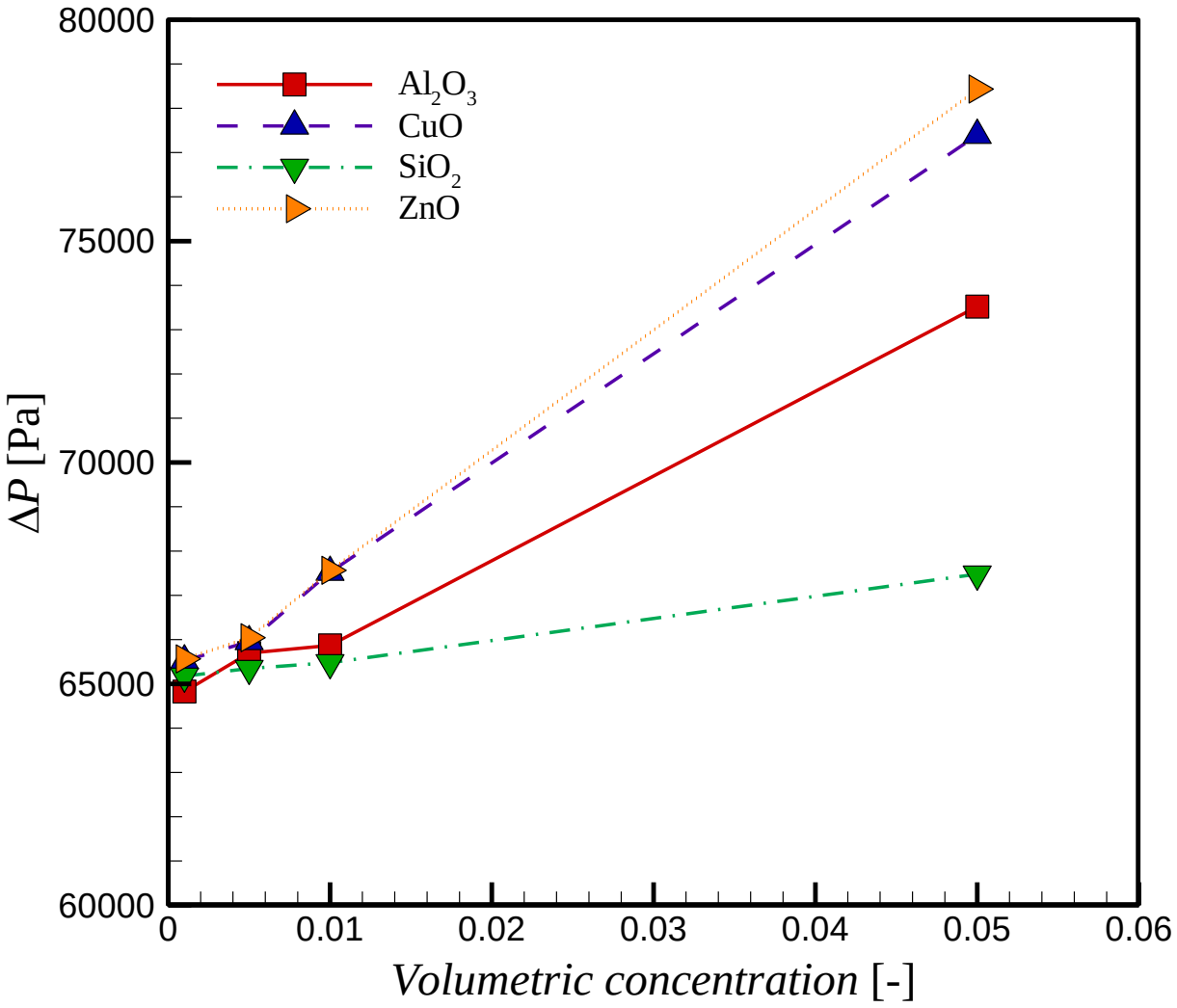

Figure 14. Effect of the nanoparticle volumetric concentration on the pressure drops of Al_2O_3-water, CuO-water, SiO_2-water, and ZnO-water nanofluids when the nanoparticle diameter is 100 nm.

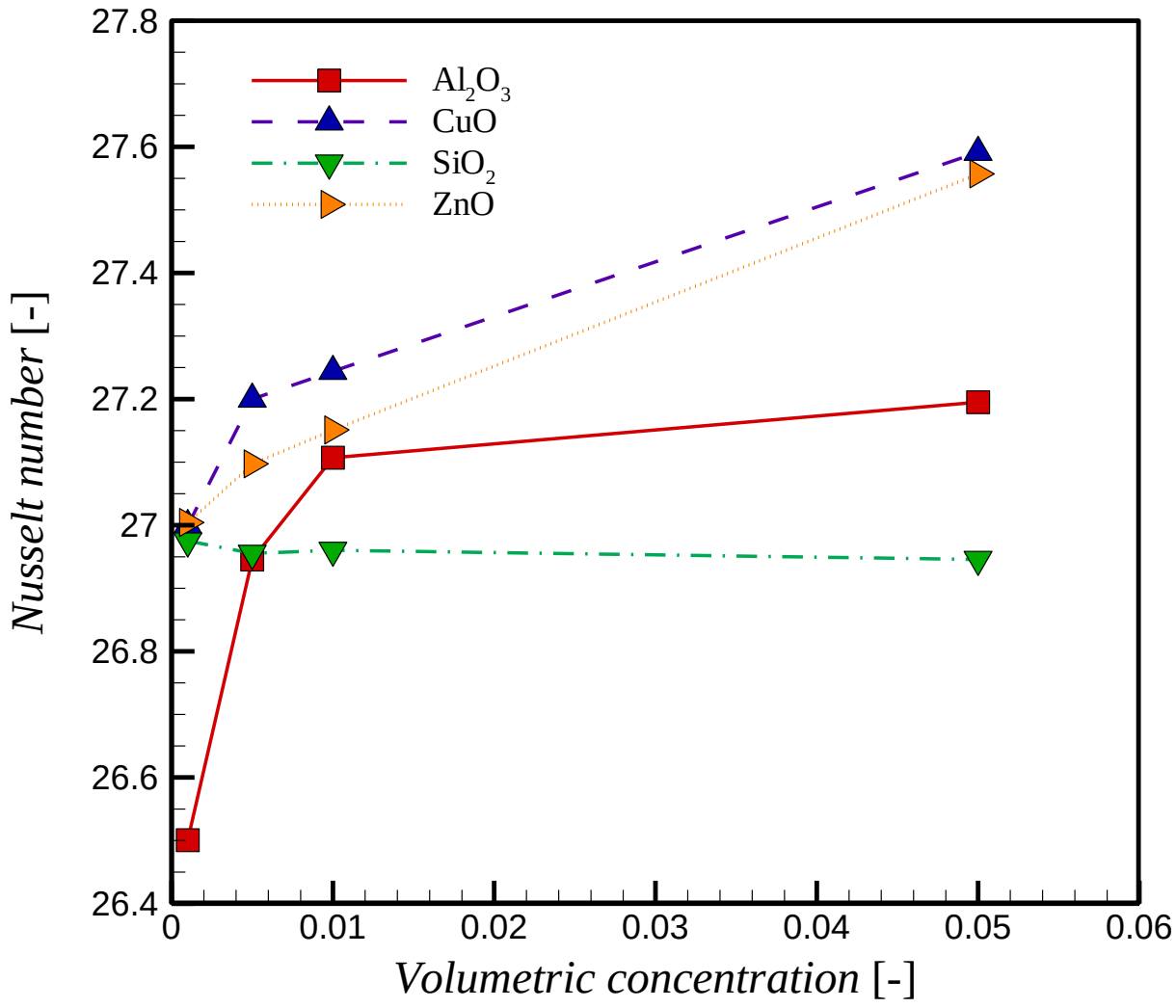

Figure 15. Effect of the nanoparticle volumetric concentration on the Nusselt numbers of Al_2O_3-water, CuO-water, SiO_2-water, and ZnO-water nanofluids when the nanoparticle diameter is 100 nm.

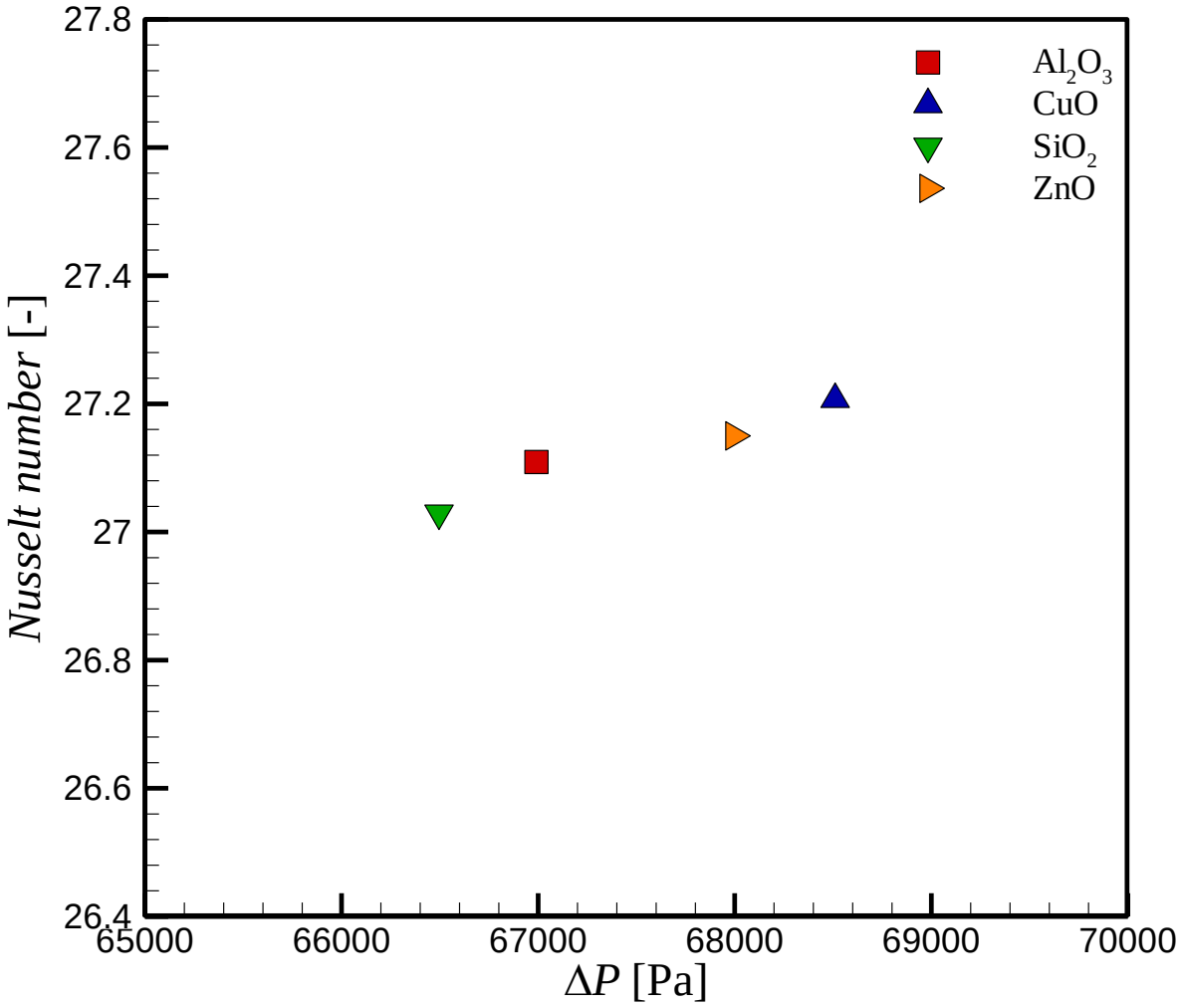

Figure 16. Effect of the choice of nanoparticle on the Nusselt number and pressure drop of nanofluids when the base fluid is water, nanoparticle diameter is 100 nm and the volumetric concentration is 1%.

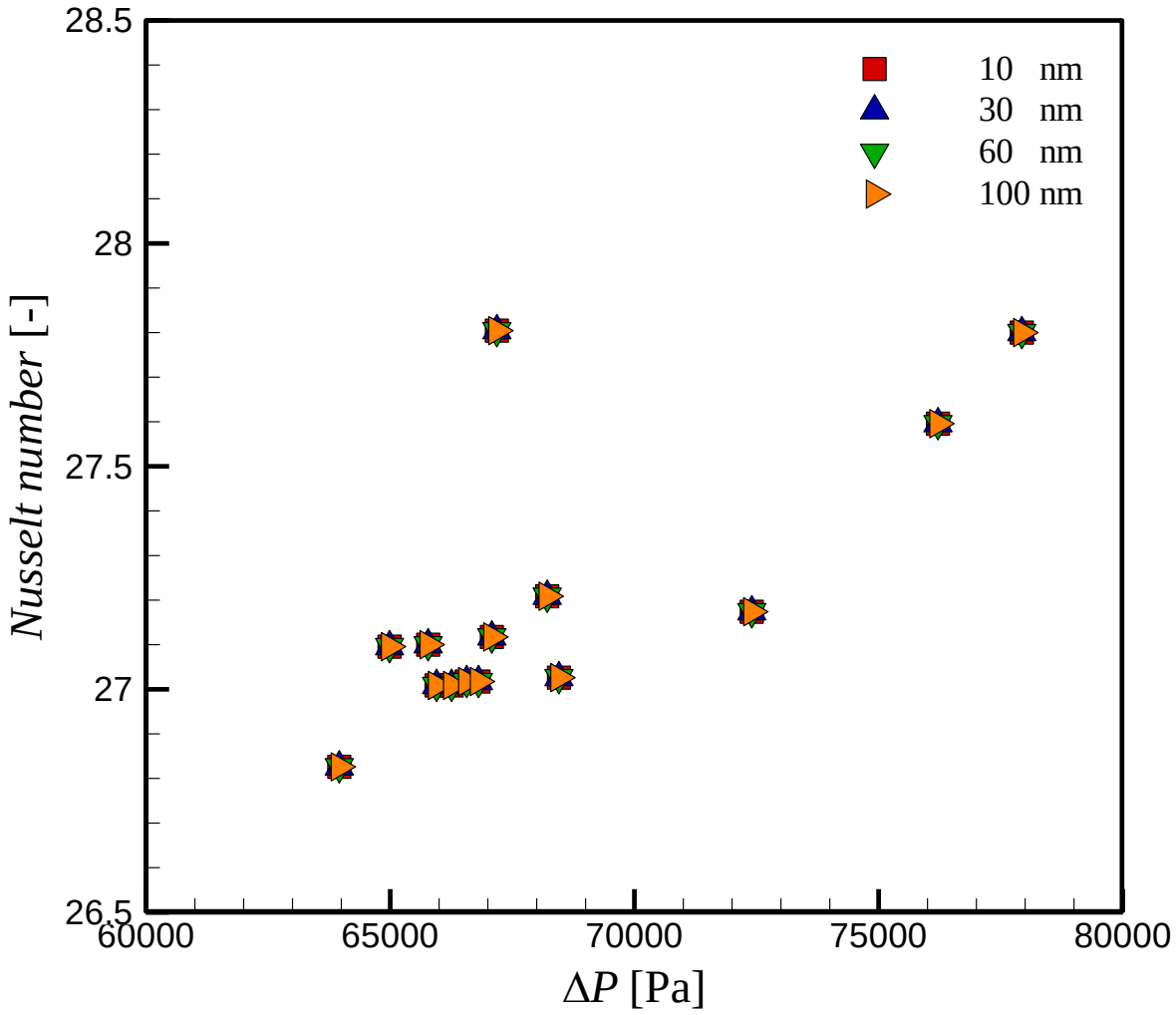

Figure 17. Effect of the nanoparticle diameters on the Nusselt number and pressure drop of nanofluids for different base fluids.

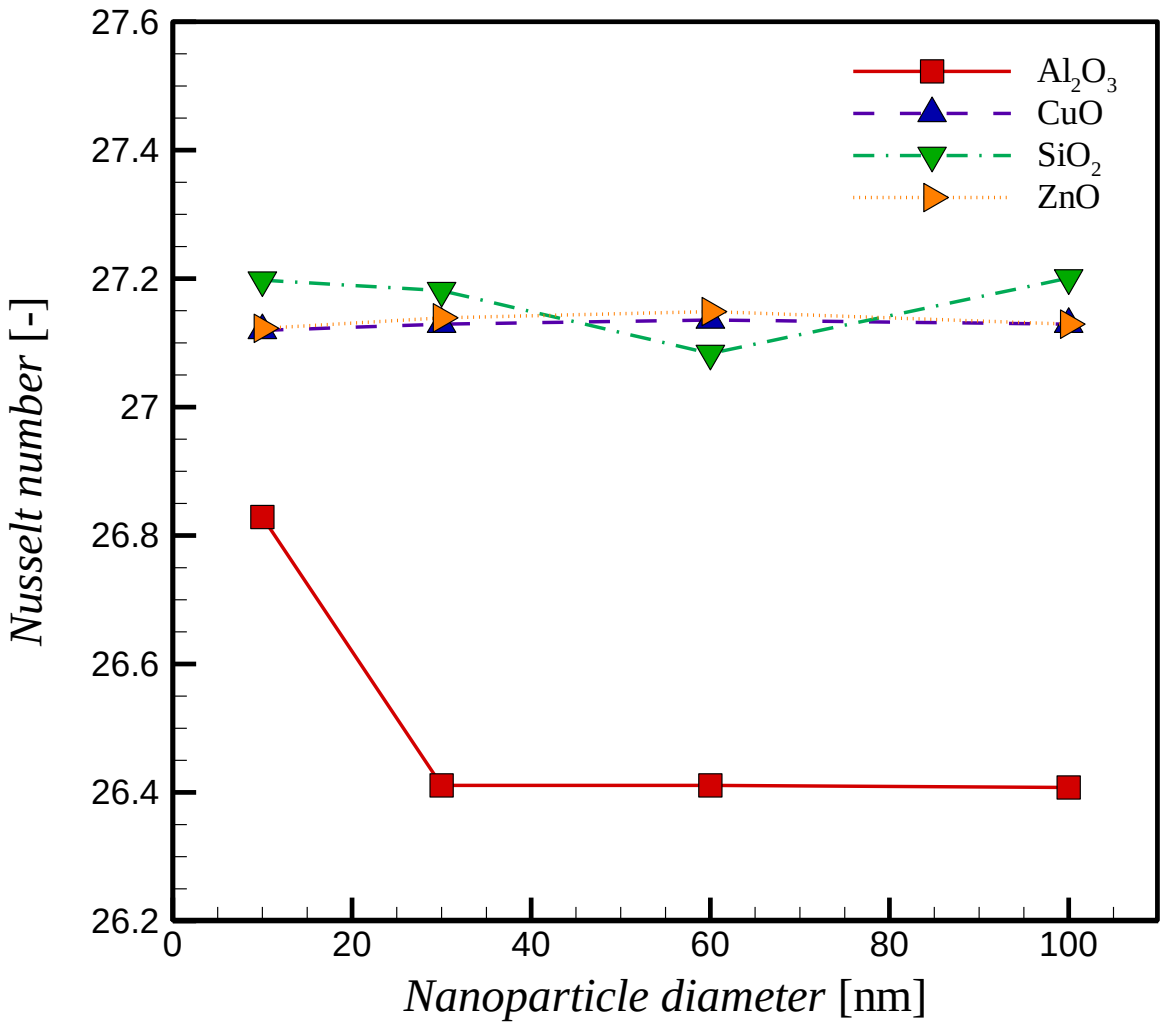

Figure 18. Effect of the nanoparticle diameters on the Nusselt numbers of Al_2O_3-water, CuO-water, SiO_2-water, and ZnO-water nanofluids.

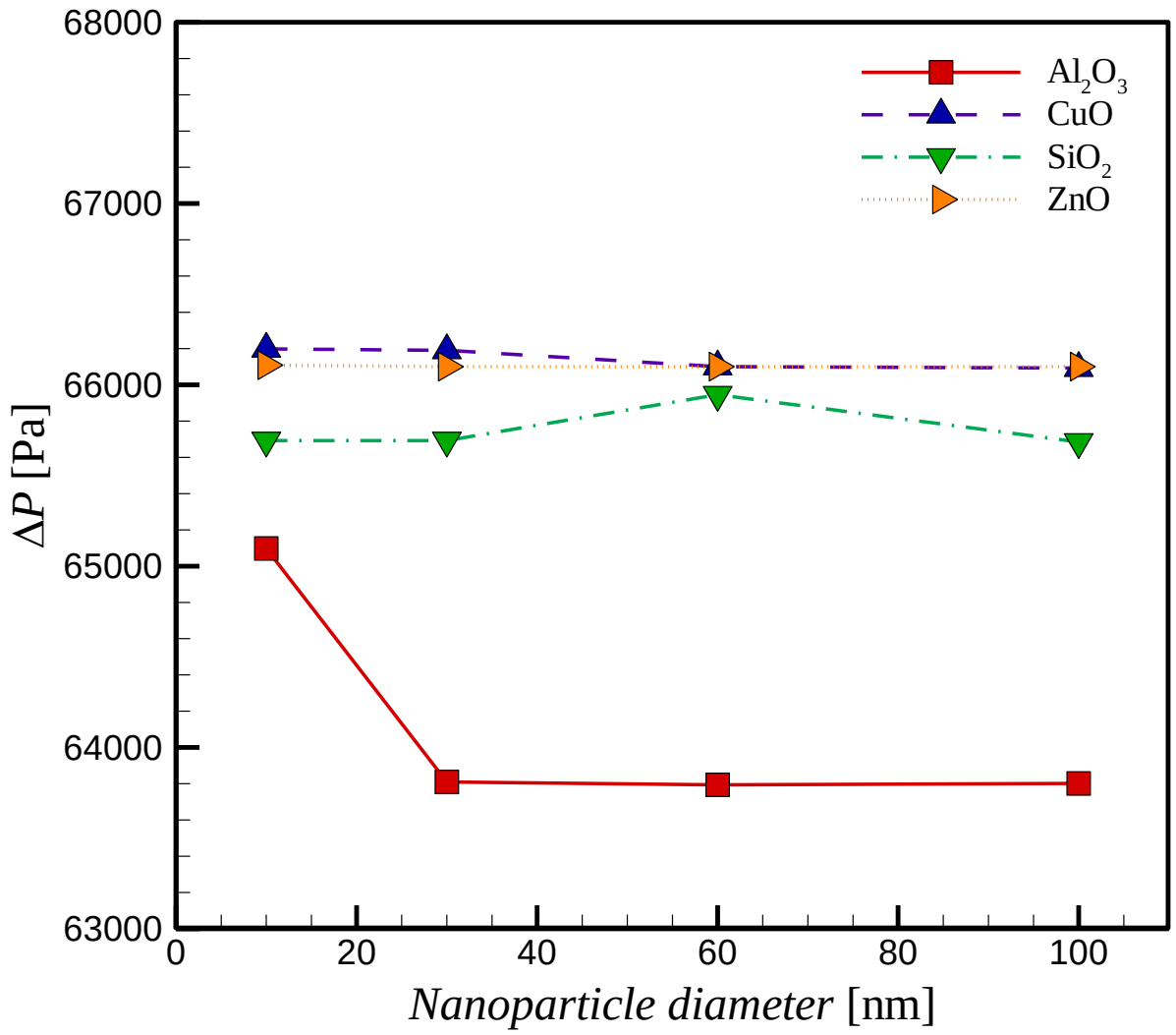

Figure 19. Effect of the nanoparticle diameters on the pressure drops of Al_2O_3-water, CuO-water, SiO_2-water, and ZnO-water nanofluids.

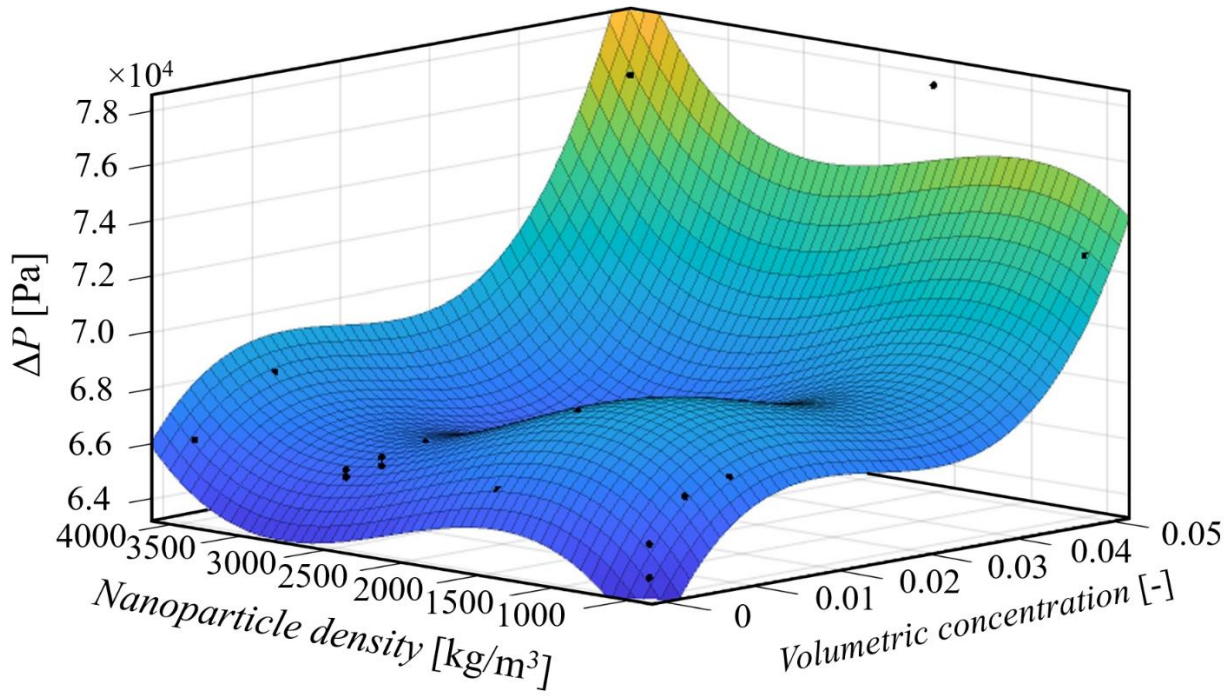

Figure 20. RBF of the pressure drop for different nanoparticles and volumetric concentrations.

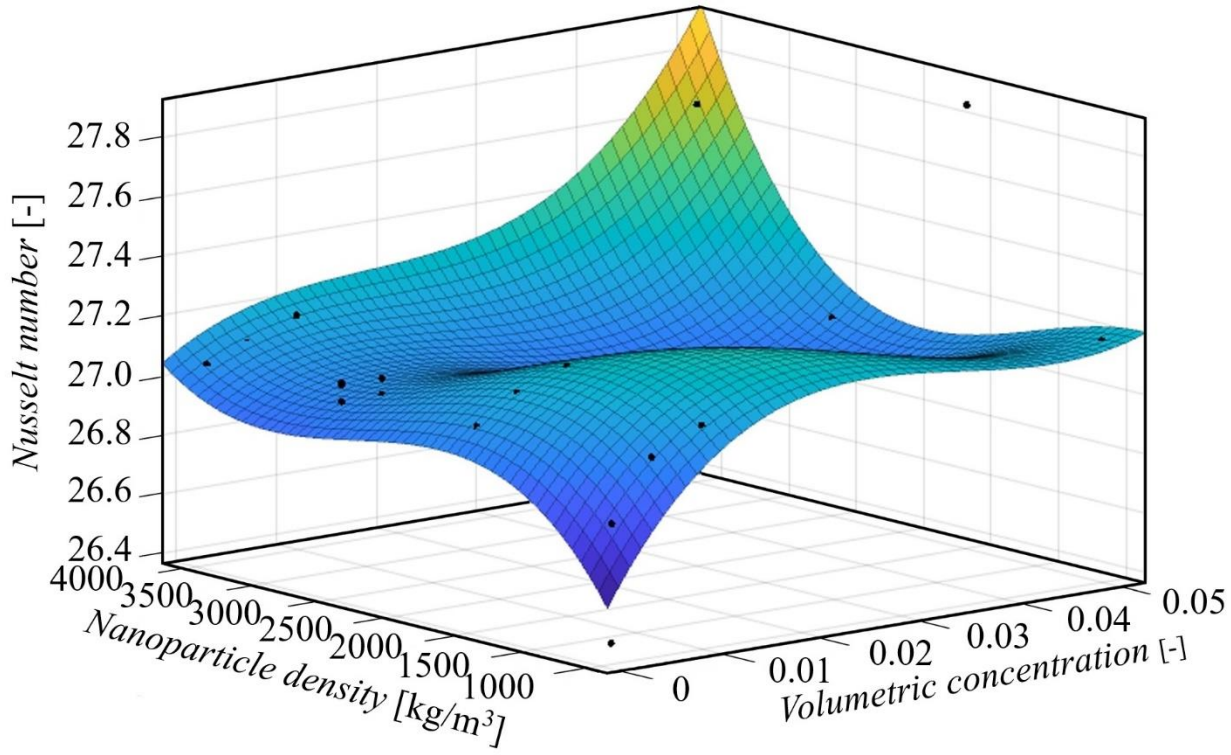

Figure 21. RBF of the Nusselt number for different nanoparticles and volumetric concentrations.

Notes on contributors

Marcel Meyer obtained his BEng in Mechanical Engineering from the University of Pretoria in 2017 and his MEng in Mechanical Engineering in 2019 from the University of Pretoria. He is a member of the Clean Energy Research Group and his research interests include nanofluids, optimisation techniques and modelling of heat and mass transfer systems.

Mehdi Mehrabi is a senior lecturer in the Department of Mechanical and Aeronautical Engineering and a member of the Clean Energy Research Group at the University of Pretoria. His research interests include heat transfer and fluid mechanics, CFD, microfluidics and their applications in the field of biomedical engineering, and modelling and optimisation based on artificial intelligence techniques. He also applies the machine and deep learning methods in the mechanical and biomedical engineering field. He has successfully supervised more than 50 undergraduate and postgraduate students at the University of Pretoria and regularly serves as a member of the examination committee for master's and PhD candidates. He received a Y1 rating from the NRF in 2020.

Josua P. Meyer is Professor and Head of the Department of Mechanical and Aeronautical Engineering and Chair of the School of Engineering at the University of Pretoria. His research field is convective heat transfer in which he has published more than 600 scholarly articles, conference papers and book chapters. He has successfully supervised more than 100 postgraduate students for research master's and PhDs. He has received various international awards for his research. According to the Essential Science Indicators of the ISI Web of Knowledge, he is ranked among the top 1% of the world in engineering in all three evaluation fields, which are citations, number of papers and citations per paper. He is/was the editor, lead editor and associate editor of various prominent international heat transfer journals.